Documentation for the Skeletal Storage, Compaction, and Subsidence (CSUB) Package of MODFLOW 6

Chapter 62 of
Section A, Groundwater
Book 6, Modeling Techniques

Techniques and Methods 6–A62

U.S. Department of the Interior
U.S. Geological Survey

Documentation for the Skeletal Storage, Compaction, and Subsidence (CSUB) Package of MODFLOW 6

By Joseph D. Hughes, Stanley A. Leake, Devin L. Galloway, and Jeremy T. White

Chapter 62 of
Section A, Groundwater
Book 6, Modeling Techniques

U.S. Department of the Interior
U.S. Geological Survey

U.S. Geological Survey, Reston, Virginia: 2022

For more information on the USGS—the Federal source for science about the Earth, its natural and living resources, natural hazards, and the environment—visit https://www.usgs.gov or call 1–888–ASK–USGS.

For an overview of USGS information products, including maps, imagery, and publications, visit https://store.usgs.gov/.

Any use of trade, firm, or product names is for descriptive purposes only and does not imply endorsement by the U.S. Government.

Although this information product, for the most part, is in the public domain, it also may contain copyrighted materials as noted in the text. Permission to reproduce copyrighted items must be secured from the copyright owner.

Preface

This report describes the skeletal storage, compaction, and subsidence (CSUB) Package of the Groundwater Flow Model for the U.S. Geological Survey (USGS) modular hydrologic simulation program, called MODFLOW 6. The MODFLOW 6 program can be be downloaded from the USGS for free. The performance of the CSUB package has been tested in a variety of applications. Future applications, however, might reveal errors that were not detected in the test simulations. Users are requested to send notification of any errors found in this model documentation report or in the model program to the MODFLOW contact listed on the Web page. Updates might be made to both the report and to the model program. Users can check for updates on the MODFLOW Web page (https://doi.org/10.5066/F76Q1VQV).

Acknowledgments

Contents

Figures

Tables

Blank page

Documentation for the Skeletal Storage, Compaction, and Subsidence (CSUB) Package of MODFLOW 6

By Joseph D. Hughes,[1] Stanley A. Leake,[2] Devin L. Galloway,[1] and Jeremy T. White[3]

Abstract

This report describes the skeletal storage, compaction and subsidence (CSUB) package of MODFLOW 6. The CSUB package simulates the vertical compaction of compressible sediments and land subsidence. The package simulates groundwater storage changes and elastic compaction in coarse-grained aquifer sediments. The CSUB package also simulates groundwater storage changes and elastic and inelastic compaction in fine-grained, compressible interbeds, or in extensive confining units. The package can account for effective stress-dependent changes in storage properties. The CSUB package can also explicitly account for the contribution of water compressibility to groundwater storage changes.

Compaction of compressible sediments is formulated using Terzaghi's elastoplastic model and assumes the total compaction is a small fraction of the total initial thickness of compressible sediments. Compaction is controlled by head or pore-pressure changes and overburden stress changes associated with water-table changes, and thus by effective stress changes within coarse- and fine-grained compressible sediments. If the stress in a compressible unit is less than the preconsolidation stress, compaction is elastic (recoverable). If the stress in a compressible sediment is greater than the preconsolidation stress, compaction is inelastic (irrecoverable) and permanent land subsidence occurs.

The propagation of head changes within fine-grained, compressible interbeds is represented numerically using a transient, one-dimensional (vertical) groundwater flow equation. This equation accounts for delayed release of water from storage or uptake of water into storage in the interbeds. Vertical hydraulic conductivity, elastic and inelastic skeletal specific storage, and interbed thickness control the timing of interbed storage changes. Interbeds that are thin, have a relatively large vertical hydraulic conductivity, or relatively small specific-storage values equilibrate quickly with heads/pore pressures in surrounding coarse-grained sediments and can be represented as no-delay interbeds that use the simulated groundwater head in a cell to calculate interbed compaction and do not need to be solved numerically using a vertically discretized interbed and the vertical groundwater flow equation.

In addition to the applicability to confined groundwater flow systems, several features of the CSUB package make it applicable to shallow, unconfined groundwater flow systems. Geostatic stress can be treated as a function of water-table elevation, and compaction is a function of computed changes in effective stress. The porosity, void ratio, and thickness of shallow and deep coarse-grained aquifer sediments, fine-grained interbeds, and extensive confining units can vary in time based on calculated strain.

---

[1]U.S. Geological Survey.

[2]Retired, U.S. Geological Survey.

[3]U.S. Geological Survey. Current affiliation: INTERA Incorporated, Boulder, Colorado.

Introduction

Land subsidence is a sudden sinking or gradual settling of the Earth's surface. Of the many causes, natural and anthropogenic, one of the principal anthropogenic causes is the compaction of susceptible aquifer systems caused by groundwater depletion (Galloway and others, 1999; Galloway and Burbey, 2011). Compressible fine-grained sediments are susceptible to inelastic compaction in response to groundwater withdrawals in many aquifer systems worldwide. Inelastic compaction of the fine-grained sediments results in largely permanent land subsidence, damaging infrastructure and increasing the frequency and intensity of flooding. The adverse effects of inelastic compaction resulting from groundwater withdrawals have been documented in many unconsolidated, heterogeneous aquifer systems, including the Central Valley in California, USA (Faunt and others, 2016); the Houston-Galveston region in Texas, USA (Kasmarek and Johnson, 2013); the Ganges-Brahmaputra Delta, Bangladesh (Alam, 1996); the Jakarta basin, Indonesia (Abidin and others, 2015); the lower Mekong Delta, Cambodia and Vietnam (Minderhoud and others, 2017); and the Virginia Coastal Plain, USA (Eggleston and Pope, 2013).

Land subsidence attributable to the compaction of aquifer systems is an often overlooked hazard and an environmental consequence of groundwater withdrawal in many areas (Galloway and others, 1999). The arid Southwestern United States is especially vulnerable because surface-water supplies are limited, and groundwater in unconsolidated basin-fill deposits is extensively relied upon (Faunt and others, 2016). Coastal regions also are commonly affected because they are often underlain by unconsolidated, compressible coastal-plain and shallow-marine sediments (Eggleston and Pope, 2013; Kasmarek and Johnson, 2013; Ingebritsen and Galloway, 2014; Shirzaei and others, 2020). Some of the hazards and environmental consequences include damage to engineered structures (such as buildings, roadways, pipelines, aqueducts, water and wastewater systems, and well casings), earth fissures, enhanced riverine or coastal flooding, loss of saltwater- and freshwater-marsh ecosystems, and reactivation of surface faults (Galloway and Burbey, 2011). Earth fissures and reactivated surface faults also create new potential pathways for surface runoff to contaminate aquifers.

For purposes of this report, the term "compaction" refers to the change in vertical thickness that accompanies changing stresses within the aquifer system, the term "aquifer" refers to a laterally extensive water-bearing unit, the term "confining unit" refers to laterally extensive fine-grained sediments separating aquifers, the term "interbeds" refers to fine-grained sediments contained in an aquifer, and the term "aquifer system" refers to a group of aquifers, possibly with interbeds, and confining units. A decrease in thickness of an aquifer system is referred to as a positive value of compaction and an increase as a negative value. All aquifer systems undergo some degree of deformation in response to changes in stress. Recharge from rainfall and natural discharge from unconsolidated heterogeneous aquifer systems typically causes measurable elastic (recoverable) compaction (Riley, 1969; Poland and Ireland, 1985; Wilson and Gorelick, 1996; Heywood, 1998) and commensurate uplift and subsidence (millimeters to centimeters) of the land surface (Amelung and others, 1999; Bawden and others, 2001; Hoffmann and others, 2001; Lu and Danskin, 2001; Sneed and others, 2014, 2018). Removing water from storage in the fine-grained silts and clays in the aquifer system cause these compressible sediments to compact, resulting in land subsidence. Fine-grained interbeds and confining units within or adjacent to unconsolidated aquifers that undergo head changes related to the development of the groundwater resource are particularly susceptible to compaction.

An example of an aquifer system composed of two aquifers, containing fine-grained interbeds, separated by a confining unit is shown in figure 1. As groundwater is drained from the fine-grained interbeds and confining units to the coarser grained sediments that constitute the aquifers, compaction can occur elastically (recoverable) or inelastically (non-recoverable) causing permanent subsidence, depending on the stress history of the interbeds and confining units. When an unconsolidated heterogeneous aquifer system is developed as a groundwater resource, most of the groundwater produced comes initially from storage in the aquifers, the more permeable interbeds, and the fringes of thicker interbeds and confining units. After some time, when lowered heads in the adjacent aquifers establish vertical head gradients between the aquifers and the interior parts of

the thicker or less permeable interbeds and confining units, groundwater is progressively contributed from more interior parts of the interbeds and confining units to the aquifers. When the magnitude and areal extent of the head decline in the aquifers become large, a significant fraction of the water supplied to pumping wells can be derived from groundwater released from storage in the interbeds and confining units (Poland and others, 1975).
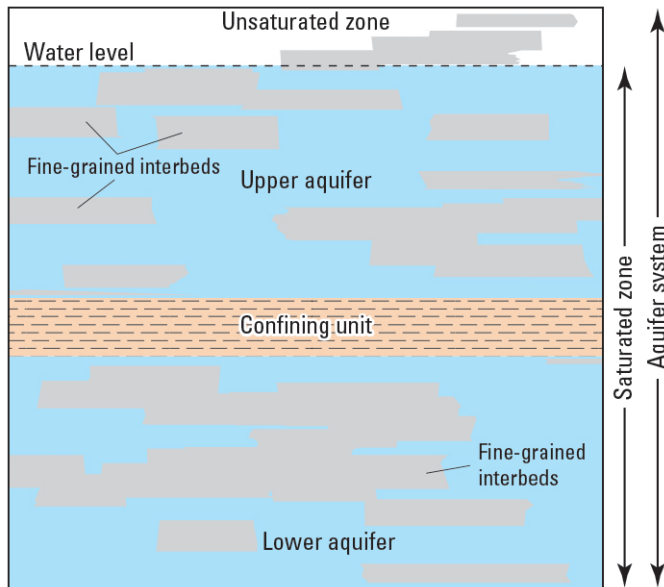
Figure 1.   Diagram showing fine-grained interbeds in an aquifer system composed of two aquifers separated by a confining unit. The fine-grained interbeds contained in the aquifers and the confining unit separating the upper and lower aquifers are susceptible to elastic and inelastic compaction. Modified from Leake and Galloway (2007).

In confined aquifer systems, the water supplied to pumping wells is derived from the compression of the sediments that constitute the matrix or granular skeleton of the aquifer system and the expansion of the water (Jacob, 1940). Matrix and water compressibility, along with porosity, determine the storativity of the aquifers and of the interbeds and confining units in the aquifer system. Typically, inelastic skeletal compressibilities (and therefore storativities) of interbeds and confining units are 1 to 2 orders of magnitude larger than elastic compressibilities of coarse-grained materials, which are typically a factor of 2 to 3 larger than water compressibility; therefore, virtually all of the water derived from interbeds and confining-unit storage is due to the compressibility of the granular skeleton. The storativities of the interbed and confining units and the drainage of these units largely govern the compaction of these aquifer systems and account for all but a negligible amount of the land subsidence that often accompanies groundwater development in these systems.

For aquifer systems that include compressible fine-grained interbeds (fig. 1), existing groundwater-model programs have been modified to account for the release of water from compacting interbeds and compute resulting compaction and land subsidence (Meyer and Carr, 1979; Williamson and others, 1989; Leake and Prudic, 1991). These computer programs keep track of the head at which the preconsolidation stress threshold will be exceeded (preconsolidation head). Values of elastic or inelastic storage coefficients are selected on the basis of a relation between the head in a model cell and the preconsolidation head. The programs are based on the assumption that elastic and inelastic skeletal specific-storage values are constant and that a unit decline in head results in a unit increase in effective stress. The Subsidence and Aquifer-System Compaction (SUB) package for the previous version of MODFLOW (MODFLOW-2005) is based on this assumption (Hoffmann and others, 2003).

Such assumptions may be appropriate for analyses of compaction in deep, confined aquifer systems but do not account for the effects of moving water tables on effective stress and the effects of stress-dependent

storage properties. These effects are likely to be most important in shallow unconfined aquifers and confining units. Several previous programs have incorporated stress-dependent storage properties. One of the programs is COMPAC1 (Helm, 1975, 1976), which simulates compaction in compressible units with specified stress changes at the boundaries. Another program, FLUMPS, (Neuman and others, 1982) calculates the compaction of confining units between model layers. Another program is the SUB-CR package for the previous version of MODFLOW (MODFLOW-2005), which simulates stress-dependent compaction based on the isotache concept, is an extension of, and incorporates the classical elastoplastic compression model of Terzaghi as a limiting case (Terzaghi, 1925; Šuklje, 1957; Kooi and others, 2018; Kooi and Erkens, 2020). And finally, the Subsidence and Aquifer-System Compaction package for Water-Table Aquifers (SUB-WT) for the previous version of MODFLOW (MODFLOW-2005), which simulates stress-dependent compaction in quickly draining compressible sediments (Leake and Galloway, 2007).

A new package was developed for the Groundwater Flow (GWF) model for MODFLOW 6 (Langevin and others, 2017), a computer program that simulates three-dimensional groundwater flow, to simulate stress-dependent aquifer-system compaction of quickly and slowly draining compressible sediments and land subsidence. The package is called the skeletal storage, compaction, and subsidence (CSUB) package or simply CSUB in this report. The CSUB package retains all of the functionality available in the SUB (Hoffmann and others, 2003) and SUB-WT (Leake and Galloway, 2007) packages for MODFLOW-2005.

Mathematical symbols used in the report are defined in appendix 1. The input-data structure for the CSUB package is described in a separate User Guide that is distributed with the MODFLOW 6 software. Example problems that demonstrate the use of the CSUB package to simulate the contribution of skeletal and interbed storage changes to groundwater flow and elastic and inelastic compaction is described in a separate MODFLOW 6 Example Problems Document that is distributed with the MODFLOW 6 software. Input files for the example problems are also included in the MODFLOW 6 software release. The MODFLOW 6 User Guide and Examples documents and CSUB package example input files are available at https://doi.org/10.5066/F76Q1VQV.

Theory

To incorporate calculations of compaction into groundwater flow models, a relation between compaction and change in groundwater head must be established. The relation presented in this report is based on Terzaghi's elastoplastic model that relates effective stress to one-dimensional compaction (Terzaghi, 1925). Compaction occurs when groundwater heads decline and the intergranular effective stress increases.

The details of the numerical implementation of Terzaghi's elastoplastic model are discussed in the following section. The assumptions and simplifications on which the mathematical representation in the CSUB package for MODFLOW 6 relies on are presented in this section. Storage coefficients are used as basic quantities to calculate head change in MODFLOW 6 and storage coefficients can be related to compaction and compression models (stresses and strains). The theory of groundwater storage is presented first and is followed by the Terzaghi (1925) theory of effective stress and stress changes. These two concepts are then combined to present the theory of one-dimensional compaction of compressible sediments. The compaction equations are developed for confined (fully-saturated) conditions but are modified to account for unconfined (water-table) conditions in the "Incorporation of skeletal storage and interbed compaction into the CVFD Groundwater Flow Equation" and "Solution of Delay Interbeds Systems" sections. The limitations resulting from these assumptions are discussed in the "Applicability and Limitations of the CSUB Package" section.

Storage

When the head in an aquifer or confining unit declines, there is a loss of storage. The hydraulic head in a piezometer open to an aquifer or confining unit is defined as

$$h = \psi + z, \tag{1}$$

where h is the hydraulic head in a piezometer open at elevation z (L), ψ is the pressure head, in terms of the elevation difference of the water column relative to the piezometer bottom (L), and z is the elevation head at the piezometer bottom (L). The pressure head is the equivalent gauge pressure of a column of water at the base of the piezometer and is defined as

$$\psi = \frac{p}{\gamma_w}, \tag{2}$$

where p is the fluid pore pressure $(ML^{-1}T^{-2})$ at elevation z and γ_w is the unit weight of water $(ML^{-2}T^{-2})$. The unit weight of water is defined as

$$\gamma_w = \rho_w g, \tag{3}$$

where ρ_w is the density of water (ML^{-3}), and g is gravitational acceleration (LT^{-2}).

Storage loss is by the dewatering of previously saturated sediments if the aquifer is unconfined and by release of stored water by the compaction of the aquifer due to the lowered fluid pore pressure (Theis, 1935; Jacob, 1940). In the saturated zone, the fluid pore pressure and the weight of overlying sediments (geostatic stress) affects the arrangement of aquifer-system materials as well as the density of water in the voids. As the fluid pore pressure decreases in a fully saturated aquifer, the aquifer materials contract; as the fluid pore pressure increases in a fully saturated aquifer, aquifer materials expand (Freeze and Cherry, 1979; Fetter, 1988). The recoverable (reversible) expansion and contraction of the aquifer materials is referred to as elastic deformation. When the head in an aquifer or confining unit declines, the aquifer/confining unit skeleton

compresses, which reduces the effective porosity and releases water. Additional water is released as the pore water expands due to lower fluid pressure; expansion of water is generally a negligible source of water.

The specific storage is the volume of water that is added to or released from a unit volume of aquifer or confining unit per unit change in head, which can be written as

$$S_s = \gamma_w \left(\alpha + \theta \beta \right) = S_{sk} + S_{sw}, \tag{4}$$

where S_s is the specific storage (L^{-1}); α is the coefficient of compressibility (matrix compressibility) of the aquifer or confining unit skeleton ($LM^{-1}T^2$); θ is porosity (dimensionless), β is the coefficient of compressibility of water ($LM^{-1}T^2$); S_{sk} is the skeletal specific storage (L^{-1}), where $S_{sk} = \gamma_w \alpha$; and S_{sw} is the water specific storage (L^{-1}), where $S_{sw} = \gamma_w \theta \beta$. Porosity is defined as

$$\theta = \frac{V_v}{V_t} = \frac{V_v}{V_s + V_v}, \tag{5}$$

where V_v is the volume of voids in a control volume (L^3), V_t is the total volume of a control volume (L^3), and V_s is the volume of solids in a control volume (L^3).

In confined aquifers and confining units, the head may decline but the potentiometric surface remains above the top of the unit and the unit remains saturated. The storage coefficient, or storativity, is defined as

$$S = dv S_s, \tag{6}$$

where S is the storage coefficient (dimensionless) and dv is the aquifer or confining unit thickness (L). The storage coefficient represents the volume of water that an aquifer or confining unit will store or release from storage per unit surface area per unit change in head. All of the water stored or released from storage is accounted for by the compressibility of the aquifer or confining unit skeleton and the pore water.

In aquifers and confining units where the head is below the top of the unit, the saturation increases or decreases with the amount of water in storage. For water-table conditions, dv depends on head. The saturated thickness for water-table conditions is calculated as

$$dv = \begin{cases} 0 & \text{if } h < zb; \\ (h - zb) & \text{if } zb \leq h < zt; \\ (zt - zb) & \text{if } h \geq zt, \end{cases} \tag{7}$$

where zt is the top of the aquifer or confining unit (L), zb is the bottom of the aquifer or confining unit (L), and h is the head (L). When water-table conditions exist, the saturated thickness is recalculated using equation 7. If head drops below the aquifer bottom (eq. 7), the aquifer or confining unit is considered to be fully dewatered even though for gravity drainage some water is retained in the pores of the unsaturated materials.

As the head falls below the top of the aquifer or confining unit, water drains from the pore spaces. Storage change in aquifers and confining units with a water table is due to the combination of specific yield and specific storage. For an aquifer or confining unit with a water table, the storage coefficient is defined as

$$S = S_y + dvS_s, \tag{8}$$

where S_y is the specific yield (dimensionless), also known as the drainable porosity, which is the volumetric fraction of the bulk aquifer volume that a given aquifer will yield when all the water is allowed to drain out of it under the forces of gravity. Typically, for unconfined aquifers, S_y is much greater than dvS_s and thus $S \approx S_y$. The volume of water added or removed from storage in an aquifer or confining unit is defined as

$$dV_w = SAdh, \tag{9}$$

where dV_w is the volume of water added or released from storage (L^3), A is the horizontal area (L^2), and dh is the change in head in an aquifer or confining unit (L).

Effective Stress and Stress Changes

Specific storage in equation 4 is related to skeletal and water compressibility. For most hydrologically relevant problems, water compressibility can be considered constant but skeletal compressibility is actually a function of effective stress (Freeze and Cherry, 1979). The theoretical basis for the compaction of subsurface materials is based on the Terzaghi (1925) theory of one-dimensional consolidation that ignores horizontal strains and stress gradients. Compaction (consolidation) occurs when effective (intergranular) stress increases. The coupling of sediment compaction and changes in hydraulic head is based on the Terzaghi (1925) principle of effective stress

$$\sigma'_{ij} = \sigma_{ij} - \delta_{ij}p, \tag{10}$$

where σ'_{ij} is a component of the effective stress tensor ($MLT^{-2}L^{-2}$), σ_{ij} is a component of the total stress tensor ($MLT^{-2}L^{-2}$), and δ_{ij} is the Kronecker delta function (dimensionless). The total stress is given by the geostatic load of the overlying saturated and unsaturated sediments and tectonic stresses.

If the interbeds are assumed to be horizontal and laterally extensive with respect to their thickness, pore-pressure gradients within the interbeds will be primarily vertical. Assuming that the resulting strains also are primarily vertical, a one-dimensional form of equation 10 can be expressed as

$$\sigma' = \sigma - p, \tag{11}$$

where σ' is the vertical component of effective stress ($MLT^{-2}L^{-2}$) and σ is the vertical component of geostatic stress ($MLT^{-2}L^{-2}$).

In order to apply equation 11 to subsidence problems, Poland and Davis (1969) expressed geostatic stress in terms of the thickness of unsaturated and saturated sediments. The geostatic stress at a depth of interest expressed in terms of the thickness of unsaturated and saturated sediments is

$$\sigma = b_m\gamma_m + b_s\gamma_s, \tag{12}$$

where b_m is the thickness of moist/unsaturated sediments (L), γ_m is the unit weight of moist sediments above the water table ($MLT^{-2}L^{-3}$), b_s is the thickness of saturated sediments (L), and γ_s is the unit weight of saturated sediments ($MLT^{-2}L^{-3}$). The unit weight of moist sediments above the water table is calculated as

$$\gamma_m = \gamma_g \left(1 - \theta\right) + \theta_w \gamma_w, \tag{13}$$

where γ_g is the unit weight of sediments ($MLT^{-2}L^{-3}$), and θ_w is moisture content of sediments in the unsaturated zone (L^3L^{-3}). The moisture content of sediments in the unsaturated zone (θ_w) is the ratio of the volume of water to the total volume, which can vary from zero to porosity (θ). The unit weight of saturated sediments is calculated as

$$\gamma_s = \gamma_g \left(1 - \theta\right) + \theta \gamma_w. \tag{14}$$

The change in effective stress resulting from a given head change in an aquifer differs when water table (unconfined) or fully saturated (confined) conditions exist. When the aquifer is unconfined, a change in head corresponds to a change in the position of the water table. The draining or re-wetting of pore space in the zone of water-table fluctuation results in a change in the geostatic stress on sediments. Poland and Davis (1969) determined that the change in effective stress caused by a head change in an aquifer with a water table is

$$d\sigma' = -\gamma_w \left(1 - \theta + \theta_w\right) dh. \tag{15}$$

When confined conditions exist in an aquifer, the geostatic stress changes negligibly with head changes owing to the small changes in the unit weight of water associated with the expansion or compression of water. Poland and Davis (1969) determined the change in effective stress caused by a head change in a fully saturated aquifer can be approximated as

$$d\sigma' = -\gamma_w dh. \tag{16}$$

Comparison of equations 15 and 16 shows that the change in effective stress caused by a head change in an aquifer with a water table is reduced by a factor of $(1 - \theta + \theta_w)$ to that caused by an equivalent head change when the aquifer is fully saturated.

Example Stress Calculations

An example of a hypothetical aquifer system with a unconfined upper aquifer and confined aquifer separated by a confining unit is used to illustrate the relations between geostatic stress, fluid pore pressure, and effective stress and the changes in stresses caused by changing heads. The aquifer system is a total of 200 meters thick, the upper aquifer is 90 meters thick, the lower aquifer is 90 meters thick, the confining unit is 20 meters thick, and the initial head is 20 meters below land surface throughout the aquifer system (fig. 2A). This example is based on an example presented in Leake and Galloway (2007, fig. 2), which is based on a similar example in Poland and Davis (1969, figs. 1–3), and ignores groundwater flow and storage changes.

Geostatic stress and fluid pore pressure can be expressed in terms of the height of an equivalent column of water by dividing by the unit weight of water (γ_w). The effective stress in terms of the height of an equivalent column of water is

$$\hat{\sigma}' = \frac{b_m \gamma_m + b_s \gamma_s}{\gamma_w} - \frac{p}{\gamma_w} = \hat{\sigma} - \psi, \tag{17}$$

where $\hat{\sigma}'$ is the effective stress in terms of the height of an equivalent column of water (L) and $\hat{\sigma}$ is the geostatic stress in terms of the height of an equivalent column of water (L). Equation 17 in terms of the hydraulic and elevation head (eq. 1) is

$$\hat{\sigma}' = \hat{\sigma} - h + z. \tag{18}$$

The stresses for the hypothetical aquifer system are computed using a unit weight of sediments in the aquifers (γ_g) of 2.05×10^4 Newtons per cubic meter, a unit weight of sediments in the confining unit (γ_g) of 1.85×10^4 Newtons per cubic meter, a unit weight of water (γ_w) of 9.81×10^3 Newtons per cubic meter, a uniform porosity (θ) of 0.22, and a moisture content of sediments in the unsaturated zone (θ_w) of 0.10. Applying equations 13 and 14 to aquifer sediments, the calculated unit weight of moist sediments above the water table (γ_m) and saturated sediments (γ_s) are 1.70×10^4 and 1.81×10^4 Newtons per cubic meter, respectively, and $(1 - \theta + \theta_w)$ is 0.88. Similarly applying equation 14 to confining-unit sediments, the calculated unit weight of saturated sediments (γ_s) is 1.66×10^4 Newtons per cubic meter.

Initial stress conditions calculated using equation 18 and an initial head value of 20 meters below land surface are shown in figure 2B. Effective stresses in the upper and lower aquifers are also highlighted at 75 meters ($\hat{\sigma}'_a$) and 150 meters ($\hat{\sigma}'_b$) below land surface. Computed stresses at 75 (horizon a) and 150 (horizon b) meters below land surface are summarized in table 1.

Table 1. Computed stresses for the hypothetical aquifer system shown in figure 2 at 75 and 150 meters below land surface.

Depth horizon, in meters below land surface	Unsaturated thickness (b_m), in meters	Saturated thickness (b_s), in meters	Geostatic stress ($\hat{\sigma}$), in meters of water	Pressure head (ψ), in meters of water	Effective stress ($\hat{\sigma}'$), in meters of water	Effective stress change ($\Delta\hat{\sigma}'$)[†], in meters of water
Initial state						
75.00	20.00	55.00	136.35	55.00	81.35	0.00
150.00	20.00	130.00	268.97	130.00	138.97	0.00
30-meter upper aquifer head decline						
75.00	50.00	25.00	132.75	25.00	107.75	26.40
150.00	50.00	100.00	265.37	130.00	135.37	−3.60
30-meter lower aquifer head decline						
75.00	20.00	55.00	136.35	55.00	81.35	0.00
150.00	20.00	130.00	268.97	100.00	168.97	30.00

[†]relative to the initial state.

The stresses after a 30-meter lowering of the water table are shown in figure 2C and table 1 shows the computed stresses at 75 and 150 meters below land surface. The geostatic stress decreases slightly below the depth of the initial water table. The upper aquifer below the depth of the active water table, the confining unit, and the lower aquifer are affected equally by a decrease in geostatic stress. The pressure head decreases in the upper aquifer by 30 meters and is unchanged in the lower aquifer. Within the confining unit, it is assumed that full equilibrium (consolidation) has been achieved, and the hydraulic head varies linearly from 50 meters below land surface at the top to 20 meters below land surface at the bottom. Effective stress increases 26.40 meters (a factor of 0.88 times the head decrease) in the upper aquifer below the water table and decreases 3.60 meters in the lower aquifer, equivalent in magnitude to the decrease in geostatic stress in the lower aquifer. In this example, effective stress in the confining unit is unchanged at a depth of 107.75 meters below land surface, a depth equivalent to 88 percent of its thickness from the top (90 meters) to the bottom (110 meters). At
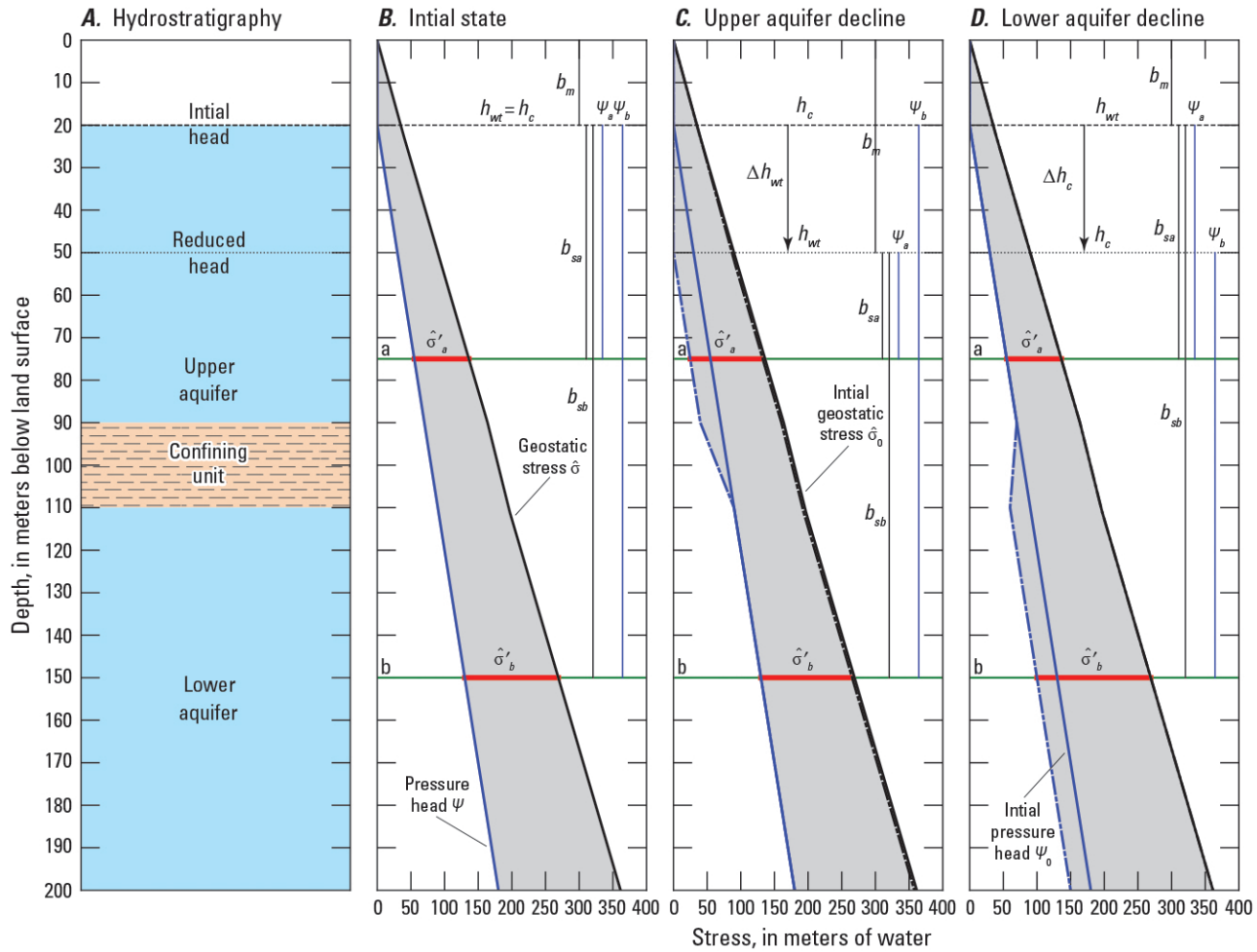
Figure 2.   Diagram showing stress diagrams for hypothetical aquifer system with head declines in an unconfined and confined aquifer. *A*, Hydrostratigraphy of the hypothetical aquifer system with an unconfined upper aquifer and a confined aquifer separated by a confining unit, *B*, initial geostatic stress, pressure head, and effective stress conditions, *C*, geostatic stress, pressure head, and effective stress conditions after a 30-meter head decline in the unconfined upper aquifer, and *D*, geostatic stress, pressure head, and effective stress conditions after a 30-meter head decline in the confined lower aquifer. The thickness of moist and saturated sediments and pressure head at points a and b are shown in *B*, *C*, and *D*. The gray area between the pressure head and geostatic stress represents the effective stress with depth. For reference, the initial geostatic stress and pressure head are shown in *C* and *D*. Modified from Leake and Galloway (2007).

this depth in the confining unit, the decrease in geostatic stress, which decreases effective stress, completely offsets the decrease in pressure head (at equilibrium), which increases the effective stress. The net change in effective stress, therefore, is zero. Above and below this depth in the confining unit, the change in effective stress is increased and decreased, respectively.

Similarly, the stresses resulting from a 30-meter lowering of hydraulic head in the lower aquifer for a static water table in the overlying unconfined upper aquifer are shown in figure 2*D*, and table 1 shows the computed stresses at 75 and 150 meters below land surface. Within the confining unit, it is assumed that the hydraulic head varies linearly from 20 meters below land surface at the top to 50 meters below land surface at the bottom. The geostatic stress is unchanged throughout the thickness of the aquifer system. The pressure head and effective stress are unchanged in the unconfined upper aquifer, and the stresses are decreased and increased by 30 meters, respectively, in the lower aquifer. Within the confining layer, under conditions of fluid-pressure equilibration, increases in effective stress vary linearly from 0 meters at the top to 30 meters at the bottom.

Compaction of Compressible Sediments

Changes in effective stress cause compaction and expansion of the sediments constituting many aquifer systems (Poland and Davis, 1969). In this report, the term "compaction" is used to describe a reduction in the thickness of compressible sediments in aquifers, confining units, and interbeds within aquifers. Conversely, the term "expansion" is used to describe an increase in the thickness of compressible sediments (negative compaction).

Void Ratio

A classical one-dimensional soil-mechanics approach (Terzaghi, 1925; Jorgensen, 1980) can be used to relate changes in the effective stress described above to compaction or expansion of sediments. For many types of sediment, the void ratio decreases linearly with increase in logarithm of effective stress. The void ratio is

$$e = \frac{V_v}{V_s} = \frac{V_v}{V_t - V_v}. \tag{19}$$

where e is the void ratio (dimensionless). The relation between void ratio and porosity is

$$e = \frac{\theta}{1 - \theta} \tag{20}$$

and

$$\theta = \frac{e}{1 + e}. \tag{21}$$

The implicit differential of equation 21 results in

$$de = (1 + e)^2 \, d\theta. \tag{22}$$

Assuming that the volume of solid material (V_s) remains constant, Jorgensen (1980) defined compaction (db) as

$$db = \frac{b}{1 - \theta} d\theta, \tag{23}$$

where b is the thickness of a control volume (L). Substituting equations 21 and 22 into equation 23 results in

$$db = \frac{b}{1 + e} de, \tag{24}$$

which is an equation used in soils engineering to describes compaction (Jorgensen, 1980). In soils engineering, compaction (and strain) is referenced to the initial conditions and modifies equation 24 to

$$db = \frac{b_0}{1 + e_0} de, \tag{25}$$

where b_0 is the initial thickness (L) and e_0 is the initial void ratio (dimensionless).

Coefficient of Compressibility

Absent horizontal displacement, Jorgensen (1980) defined a one-dimensional coefficient of compressibility in differential form as

$$\bar{\alpha} = \frac{de}{d\sigma'}, \tag{26}$$

where $\bar{\alpha}$ is the one-dimensional (vertical) coefficient of compressibility of the aquifer or confining unit (MLT^{-2}).

The coefficient of compressibility is not constant and must be determined for each condition of loading Jorgensen (1980). The compression index is related to $\bar{\alpha}$ and is equal to the slope of the closest straight line fit of a curve defined by a plot of void-ratio values versus the logarithm of the load (effective stress) of compressive material in the inelastic range. Typically, the compression curve for the elastic range (recompression index) will also define a straight line, and a coefficient can be defined for this range. Unfortunately, the compression curves for some compressible sediments do not define a straight line in either range, but the compression index is useful in describing many compressible sediments Jorgensen (1980). The compression index is defined as

$$C_c = \frac{de}{d\log_{10}\sigma'}, \tag{27}$$

where C_c is the compression index (dimensionless). The relation between $\bar{\alpha}$ and C_c for the inelastic range is defined by combining equations 26 and 27

$$\bar{\alpha} = C_c \frac{d\log_{10}\sigma'}{d\sigma'}. \tag{28}$$

The derivative of $\log_{10}\sigma'$ with respect to σ' in equation 28 is

$$\frac{d\log_{10}\sigma'}{d\sigma'} = \frac{1}{\sigma'\ln 10} = \frac{0.434}{\sigma'} \tag{29}$$

Substitution of equation 29 into equation 28 results in

$$\bar{\alpha} = \frac{0.434 C_c}{\sigma'}. \tag{30}$$

The relation between the inelastic change in the void ratio and effective stress is defined by combining equations 30 and 26

$$de_v = \frac{0.434 C_c}{\sigma'} d\sigma', \tag{31}$$

where de_v is the inelastic change in the void ratio (dimensionless). The relation between inelastic compaction and effective stress is defined by combining equations 24 and 31

$$db_v = \frac{0.434 C_c b_0}{(1 + e_0)\,\sigma'} d\sigma', \tag{32}$$

where db_v is inelastic compaction (L). Inelastic compaction is synonymous with the term "virgin consolidation" used in soil mechanics. Equation 32 is applicable for σ' values that exceed the preconsolidation stress. The preconsolidation stress corresponds to the previous maximum effective stress. For σ' values less than or equal to the preconsolidation stress, the relation between elastic compaction and effective stress is

$$db_e = \frac{0.434 C_r b_0}{(1 + e_0)\,\sigma'} d\sigma', \tag{33}$$

where db_e is elastic compaction (L) and C_r is the recompression index (dimensionless). Elastic compaction is synonymous with the term "non-virgin consolidation" used in soil mechanics. From empirical studies, C_c is much larger than C_r. Equation 32 is valid for σ' values in excess of the preconsolidation stress, and resulting changes in the void ratio (de_v) are permanent—the result of inelastic compaction.

During compaction, e and b change in response to inelastic (eq. 32) and elastic (eq. 33) compaction. However, the ratio of b to $(1 + e)$ remains constant. The ratio of b to $(1 + e)$ can be calculated using equations 5 and 19

$$\frac{b}{1 + e} = \frac{V_t}{1 + \frac{V_v}{V_t - V_v}} = \frac{V_t}{\frac{V_t - V_v + V_v}{V_t - V_v}} = \frac{V_t}{\frac{V_t}{V_t - V_v}}. \tag{34}$$

Equation 34 can be simplified to

$$\frac{b}{1 + e} = V_t - V_v = V_t - \theta V_t = 1 - \theta. \tag{35}$$

A consequence of the constant ratio of b to $(1 + e)$ is that the thickness and void ratio do not have to be updated from b_0 and e_0, respectively, when calculating inelastic (db_v) and elastic (db_e) compaction.

Leake and Prudic (1991) related db_v and db_e to $d\sigma'$ by

$$db_v = \frac{S_{skv} b_0}{\gamma_w} d\sigma', \tag{36}$$

where S_{skv} is the inelastic skeletal specific storage value (L^{-1}) and

$$db_e = \frac{S_{ske} b_0}{\gamma_w} d\sigma', \tag{37}$$

where S_{ske} is the elastic skeletal specific storage value (L^{-1}). The subscript v in S_{skv} refers to the virgin or inelastic stress range, that is for effective stresses greater than the preconsolidation stress (Jorgensen, 1980). Combining equations 32 and 36 allows S_{skv} to be expressed as

$$S_{skv} = \frac{0.434 C_c \gamma_w}{(1 + e_0)\,\sigma'}. \tag{38}$$

Similarly, combining equations 33 and 37 allows S_{ske} to be expressed as

$$S_{ske} = \frac{0.434 C_r \gamma_w}{(1 + e_0)\, \sigma'}. \tag{39}$$

Equation 38 is consistent with expressions given by Helm (1976), Jorgensen (1980), and Neuman and others (1982). Note that skeletal specific storage is inversely related to effective stress. For deep sediments, σ' will be large, and reductions in the pressure head (ψ) resulting from groundwater pumping are not likely to make large percentage changes in σ'. For that case, S_{skv} and S_{ske} can be treated as constants with little resulting error. On the other hand, for shallow sediments where σ' is relatively small, changes in the pressure head (ψ) could result in relatively large percentage changes in σ'.

A general equation for elastic and inelastic compaction or expansion of sediments can be developed by combining equations 32 and 33 for a finite effective stress change and is expressed as

$$\Delta b = \frac{0.434 b_0}{(1 + e_0)\, \sigma'^t} \left(C^t \left(\sigma'^t - \sigma'_c \right) + C_r \left(\sigma'_c - \sigma'^{t_{old}} \right) \right) \quad C^t = \begin{cases} C_c, & \sigma'^t > \sigma'_c \\ C_r, & \sigma'^t \le \sigma'_c \end{cases}, \tag{40}$$

where Δb is the compaction between time t and t_{old} (L), σ'^t is the effective stress at time t, $\sigma'^{t_{old}}$ is the effective stress at time t_{old}, and σ'_c is the preconsolidation-stress value. The relation of σ'^t to σ'_c is used to determine whether the value of C^t is C_c or C_r. The expression gives correct results for overconsolidated sediments, for normally consolidated sediments, and for sediments in transition from overconsolidation to normal consolidation (Leake and Galloway, 2007). Normally consolidated soils are soils that are currently experiencing the greatest effective stress ever experienced (preconsolidation stress) and overconsolidated soils are soils experiencing an effective stress less than the preconsolidation stress.

In cases where σ'^t is less than or equal to σ'_c, equation 40 simplifies to

$$\Delta b = \frac{0.434 b_0}{(1 + e_0)\, \sigma'^t} C_r \left(\sigma'^t - \sigma'^{t_{old}} \right), \tag{41}$$

which is the elastic storage equation in terms of effective stress instead of hydraulic head and allows for recovery of some of the compaction that occurred when the preconsolidation stress was exceeded.

Elastic and inelastic compaction or expansion of sediments is directly related to the volume of water released from or added to storage. The finite form of equations 4 and 9 with matrix compressibility in terms of effective stress and water compressibility in terms of head is

$$\Delta V_w = A \left(\Delta b + dv \gamma_w \theta \beta \Delta h \right). \tag{42}$$

Water is released from storage during compaction (positive $\Delta \sigma'$ and ΔV_w) and added to storage during expansion (negative $\Delta \sigma'$ and ΔV_w).

Void Ratio and Thickness Changes

The relation between void ratio changes (de) and compaction (db) can be determined by rearranging equation 25 to

$$de = \frac{db}{b_0}(1 + e_0) = \epsilon(1 + e_0),$$
(43)

where ϵ is total vertical strain (dimensionless). Based on the convention that compaction is a positive value, the void ratio after compaction is

$$e = e_0 - \epsilon(1 + e_0).$$
(44)

Similarly, the thickness after compaction is

$$b = b_0 - db.$$
(45)

Example Compaction Calculations

An example of a saturated clay compacting in response to a variable but generally increasing effective stress (and declining head) is used to illustrate the relation of effective stress to vertical strain in inelastic and elastic stress ranges. For this example, a 1-meter-thick interbed unit with a porosity of 0.33 (void ratio of 0.5) and compression index of 0.2 and recompression index of 0.01 is subjected to an 80 meter effective stress increase resulting from an 80-meter head decline (fig. 3A). Compression and recompression indices that exceed typical aquifer values have been used to highlight the relation of effective stress to vertical strain but result in calculated strains which exceed strains seen in aquifers. Compaction in response to effective stress changes is assumed to be instantaneous.

The clay interbed is located at the bottom of a 99-meter-thick aquifer and to simplify calculations, a constant specific gravity (γ_g/γ_w) of 1 was specified for both moist and saturated sediments. The compressible clay is exposed to periods of increasing and decreasing effective stresses that result in periods of inelastic and elastic compaction and expansion. The initial preconsolidation stress was specified to be 20 meters and the effective stress exceeds the preconsolidation stress from a fractional time of 0.28 to 0.45 and again from a fractional time of 0.96 to 1.

Inelastic and elastic compaction and associated vertical strain were calculated using equations 40 and 41. The void ratio was calculated from the calculated vertical strain using equation 44. The non-linear relation between stress and vertical strain is shown in figure 3B, and the linear relation between $\log_{10}$(stress), strain and the void ratio is shown in figure 3C. A total vertical strain of 0.18 was observed at fractional time 1 in response to the effective stress changes. Initially, the clay is overconsolidated and elastically compacts until fractional time of 0.28 when a vertical strain of 0.021 is achieved. The clay is normally consolidated from fractional time 0.28 to 0.45 and compacts an additional 0.15 meters, which increases the vertical strain to 0.17. The clay becomes overconsolidated again from fractional time 0.45 to 0.96 during which an equal amount of expansion and compaction (0.021 meters) occurs before the clay becomes normally consolidated and inelastic compaction resumes. During the final period of normal consolidation (from fractional time of 0.96 to 1) an additional 0.016 of inelastic vertical strain occurs. Vertical strain during times when the clay interbed was normally consolidated totaled 0.16 and accounted for 88.5% of the the total strain experienced. The remaining strain (experienced from fractional time 0 to 0.28) was 11.5% of the total strain. The strain experienced when the clay was overconsolidated and the recoverable portion of strain experienced when the clay was normally consolidated could be recovered if effective stress values decreased and remained less than the effective stress at fractional time 1.
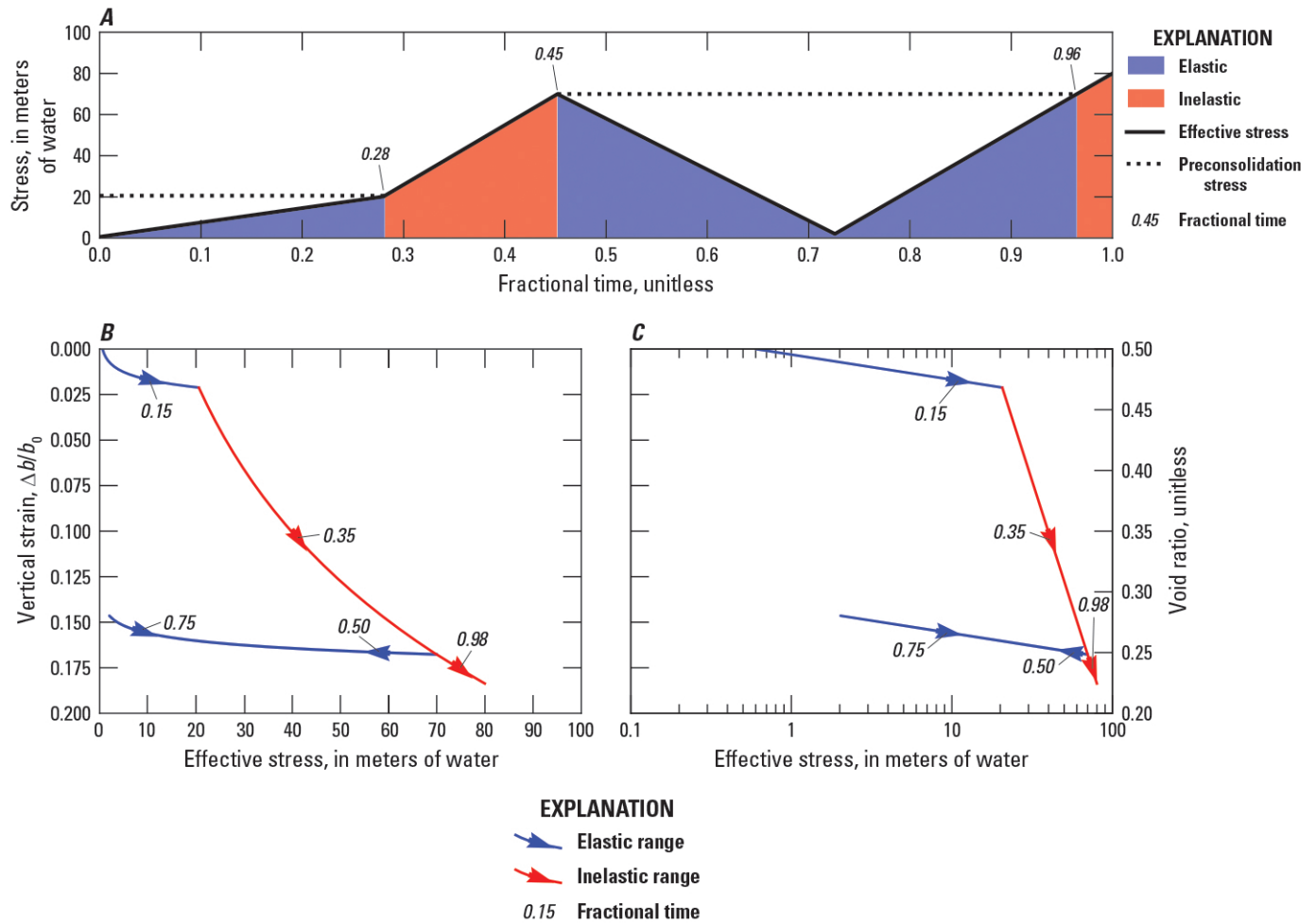
Figure 3.   Diagram showing an idealized stress-strain relation for a saturated compacting thick interbed. *A*, effective-stress conditions and related preconsolidation stress conditions; *B*, illustration of the non-linear stress-strain relation and associated void ratio for the effective-stress conditions shown in *A*; and *C*, illustration of the linear $\log_{10}$(stress)-strain relation and associated void ratio for the effective-stress conditions shown in *A*. Note the red vertical strain line identified on *B* and *C* corresponds to times when the effective-stress exceeds the preconsolidation stress shown in *A*. Select fractional times are shown in *B* and *C* and the trajectories of the elastic and inelastic curves corresponding to the select fractional times are shown in *B*.

Computing Skeletal and Interbed Storage Changes and Compaction

The CSUB package replaces the standard specific storage formulation in the MODFLOW 6 storage (STO) package with a more comprehensive stress-dependent storage formulation. The CSUB package adds storage terms to the control-volume finite-difference (CVFD) equations that represent the effect of inelastic- and elastic-storage and water compressibility in a model cell on groundwater flow. Storage changes calculated by the CSUB package are then used to calculate compaction and expansion of compressible sediments. Additional information on the formulation of the standard MODFLOW 6 packages used to approximate the three-dimensional groundwater flow equation and solution of the CVFD equations can be found in Langevin and others (2017) and Hughes and others (2017), respectively.

Stress Calculations and Basic Assumptions

In the CSUB package, coarse-grained sediments that can experience elastic compaction and fine-grained interbeds that can experience elastic and inelastic compaction are assumed to be uniformly distributed throughout the entire thickness of a control volume that we designate as a GWF model cell n. Furthermore, in MODFLOW 6 it is assumed that there is a single value of head (h_n) in the GWF cell n at time t.

Stress quantities are specified and internally calculated in MODFLOW 6 as an equivalent height of water to simplify interpretation of model results and are denoted with a $\wedge$ superscript over the geostatic stress ($\hat{\sigma}$), effective stress ($\hat{\sigma}'$), and preconsolidation stress ($\hat{\sigma}'_c$) variables. Geostatic stress, pressure head, and effective stress calculations are made for every active cell in a MODFLOW 6 model. The stress calculations made for each active cell are referenced to the bottom of each active cell (zb) and are calculated from the topmost cells to the lowermost cells in a model. Effective stress changes used to calculate storage changes are referenced to the bottom of each cell but the effective stress at the center of the saturated thickness of a model cell is used to calculate average elastic- and inelastic-specific storage values for each cell.

Geostatic Stress

The geostatic stress at the bottom of cell n, based on equation 18, is calculated as

$$\hat{\sigma}_n = \bar{\sigma}_o + b_{m_n} G_{m_n} + b_{s_n} G_{s_n}, \tag{46}$$

where $\bar{\sigma}_o$ is the average geostatic stress in the cells directly overlying cell n in terms of the height of an equivalent column of water (L), G_m is the specific gravity of moist sediments in cell n (dimensionless), and G_s is the specific gravity of saturated sediments in cell n (dimensionless). Equation 46 allows for water-table conditions in any cell, not just the uppermost cells, and is consistent with the formulation of the MODFLOW 6 node property (NPF) and STO Packages (Langevin and others, 2017). The specific gravity of moist sediments in cell n is

$$G_{m_n} = \frac{\gamma_{m_n}}{\gamma_w}, \tag{47}$$

and the specific gravity of saturated sediments in cell n is

$$G_{s_n} = \frac{\gamma_{s_n}}{\gamma_w}. \tag{48}$$

The thickness of moist/unsaturated sediments in cell n is

$$b_{m_n} = \begin{cases} 0 & \text{for } h_n \geq zt_n \\ zt_n - \bar{h}_n & \text{for } h_n < zt_n \end{cases},$$ (49)

where $\bar{h}$ is a linear corrected head (L) that transitions between the head in cell n and the bottom of the cell. The thickness of saturated sediments in cell n is

$$b_{s_n} = \begin{cases} zt_n - zb_n & \text{for } h_n \geq zt_n \\ \bar{h}_n - zb_n & \text{for } h_n < zt_n \end{cases}.$$ (50)

The linear corrected head is calculated as

$$\bar{h}_n = \begin{cases} h_n & \text{for } h_n \geq zb_n \\ zb_n & \text{for } h_n < zb_n \end{cases}.$$ (51)

If cell n has no overlying cell, $\bar{\sigma}_o$ is set to 0 or a specified load applied to a cell with no overlying cells; in this case, $\bar{\sigma}_o$ could represent the geostatic load of aquifer sediments above those represented in the model or an applied load (for example, the load associated with a large urban area overlying a model cell or cells). For the case where the horizontal extent of cell n is coincident with or contained within overlying cell m, $\bar{\sigma}_o$ is equal to $\hat{\sigma}_m$. To illustrate the case where the horizontal extent of cell n is the same as overlying cell m, consider an aquifer system with two 50-meter-thick aquifers, water-table elevations of 75 and 15 meters, a G_n value of 1.7, and a G_s value of 2.0 (fig. 4A). For this case, $\bar{\sigma}_o$ is equal to $\hat{\sigma}_m$ (92.5 meters) and $\hat{\sigma}$ at the bottom of cell n is 182.0 meters. For the case with finer horizontal discretization in the lower aquifer and the same water-table elevation in the upper aquifer (75 meters), $\bar{\sigma}_o$ is also equal to $\hat{\sigma}_m$ (92.5 meters); the two cells in the lower aquifer, however, have $\hat{\sigma}$ values at the bottom of cell n and $n+1$ equal to 185 and 179 meters since water-table elevations are 25 and 5 meters, respectively (fig. 4B).

In the case where a model is discretized using an unstructured grid and cell n has one or more overlying cells, $\bar{\sigma}_o$ is the average geostatic stress in the cells directly overlying cell n and is calculated as

$$\bar{\sigma}_o = \frac{1}{A_n} \sum_{\substack{m \in \eta_n \\ zb_m = zt_n}} \hat{\sigma}_m A_{(n,m)},$$ (52)

where η_n are the cells connected to cell n and $A_{(n,m)}$ is the overlapping area for the connection between cells n and m (L^2). Application of equation 52 to the case where the upper aquifer of the two-aquifer system presented previously has increased horizontal resolution, $\bar{\sigma}_o$ (92.5 meters) is equal to the average of $\hat{\sigma}_m$ (95.5 meters) and $\hat{\sigma}_{m+1}$ (89.5 meters) and $\hat{\sigma}$ at the bottom of cell n is 182.0 meters (fig. 4C).

Pressure Head

The pressure head at the bottom of cell n, based on equation 1, is calculated as

$$\psi_n = \bar{h}_n - zb_n.$$ (53)
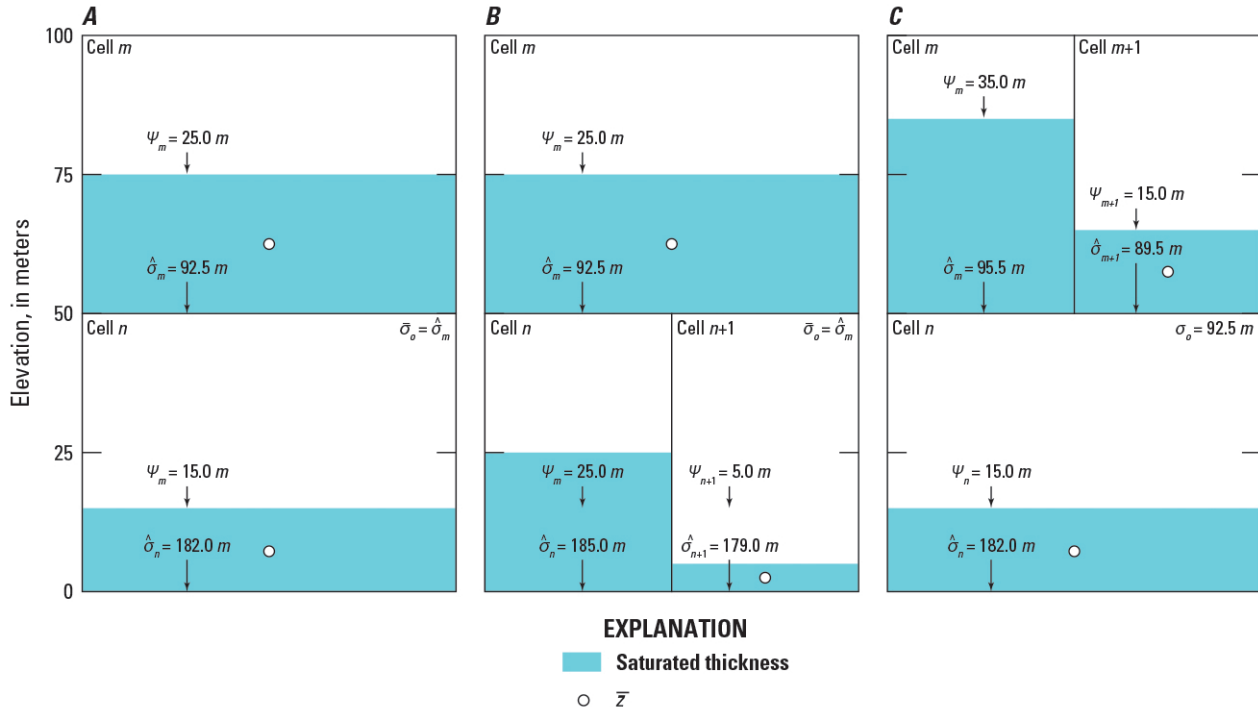
Figure 4. Diagram showing geostatic stresses ($\hat{\sigma}$), pressure heads (ψ), and the center of the saturated thickness ($\bar{z}_n$) for cells in two aquifers and the average geostatic stresses ($\bar{\sigma}_o$) at the bottom of the upper aquifer using different horizontal discretizations. *A*, geostatic stress and pressure head at the bottom of each cell and the average geostatic stress at the bottom of the upper aquifer; *B*, geostatic stress and pressure head at the bottom of each cell and average geostatic stress at the bottom of the upper aquifer for the case where the lower aquifer has increased horizontal resolution; and *C*, geostatic stress and pressure head at the bottom of each cell and average geostatic stress at the bottom of the upper aquifer for the case where the upper aquifer has increased horizontal resolution.

The pressure heads at the bottom of each cell in the 100-meter aquifer system presented earlier to demonstrate calculation of $\hat{\sigma}$ and $\bar{\sigma}_o$ for different horizontal resolutions and water-table elevations are shown in figure 4.

Effective Stress

The effective stress at the bottom of cell n, based on equation 18, in terms of the height of an equivalent column of water is calculated as

$$\hat{\sigma}'_n = \hat{\sigma}_n - \bar{h}_n + zb_n. \tag{54}$$

Combining equations 46, 49, 50, and 53 results in

$$\hat{\sigma}'_n = \begin{cases} \bar{\sigma}_o + (zt_n - zb_n)\, G_{s_n} - \bar{h}_n + zb_n & \text{for } h_n \geq zt_n \\[2ex] \bar{\sigma}_o + (zt_n - \bar{h}_n)\, G_{m_n} + (\bar{h}_n - zb_n)\, G_{s_n} - \bar{h}_n + zb_n & \text{for } h_n < zt_n \end{cases}. \tag{55}$$

The elevation of the center of the saturated thickness in model cell n is used in the calculation of effective stress in the denominator of the inelastic and elastic skeletal specific storage equations (eqs. 38 and 39). For this value, the CSUB package computes effective stress from geostatic stress and pore pressure at the center

of the saturated thickness in a cell. The cell center elevation (the center of the saturated interval in a cell) is computed from head and cell bottom elevations. For cells that do not contain a water table (fully saturated), the cell center is a fixed reference point halfway between the top and bottom of the cell. For cells that contain a water table, the elevation of the center of the saturated interval changes by half the amount of any change in the water table. Specific-storage values calculated using the elevation of the center of the saturated thickness in model cell n can be thought of as the average storage coefficient of the saturated portion of the cell.

The effective stress at the bottom of the cell is adjusted to the center of the saturated thickness in a model cell using

$$\bar{\sigma}'_n = \hat{\sigma}'_n - (\bar{z}_n - zb_n)(G_{s_n} - 1), \tag{56}$$

where $\bar{\sigma}'$ is the average effective stress, in terms of the height of an equivalent column of water, used in the inelastic and elastic skeletal specific storage equations (L) and $\bar{z}_n$ is the center of the saturated thickness in cell n (L). The center of the saturated thickness is calculated as

$$\bar{z}_n = \begin{cases} \dfrac{1}{2}(zt_n + zb_n) & \text{for } h_n \geq zt_n \\ \dfrac{1}{2}(\bar{h}_n + zb_n) & \text{for } h_n < zt_n \end{cases}. \tag{57}$$

Substituting equation 57 into equation 56 results in

$$\bar{\sigma}'_n = \begin{cases} \hat{\sigma}'_n - \dfrac{1}{2}(zt_n - zb_n)(G_{s_n} - 1) & \text{for } h_n \geq zt_n \\ \hat{\sigma}'_n - \dfrac{1}{2}(\bar{h}_n - zb_n)(G_{s_n} - 1) & \text{for } h_n < zt_n \end{cases}. \tag{58}$$

The center of the saturated thickness in each cell $(\bar{z})$ for the 100-meter aquifer system presented earlier to demonstrate the calculation of $\hat{\sigma}$, $\bar{\sigma}_o$, and ψ for different horizontal resolutions and water-table elevations is shown in figure 4.

Leake and Galloway (2007) used the average effective stress from the previous time step to reduce the non-linearity of the effective stress formulation. Computing storage properties using the effective stress from the previous time step is different from the approach used for the MODFLOW 6 storage package, which uses current heads to determine storage properties for the current time step. By default, the average effective stress from the current time step is used to calculate specific-storage values in the CSUB package. Optionally, specific-storage values calculated based on the previous time step, and consistent with Leake and Galloway (2007), can be used in the CSUB package to reduce non-linearities or for comparison with models developed using previous versions of MODFLOW subsidence packages.

The elevation at the bottom of the cell is used to calculate the effective stress change and resulting storage change. Use of the cell bottom results in a fixed datum being used to calculate the effective stress change. If the elevation at the center of the saturated thickness were used to calculate the effective stress change, the effective stress for the current or previous time step would need to be corrected to the same elevation to calculate the correct effective stress change.

In general, the equations for elastic and inelastic compaction of sediments are formulated for confined aquifers. However, to accommodate water-table conditions in a given cell, an option has been included in the CSUB package to vary the thickness of compressible sediments (coarse- or fine-grained) in proportion to changes in the saturated thickness of a model cell in an unconfined aquifer. This treatment of sediment thick-

ness is analogous to varying transmissivity in response to changes in head and thereby saturated thickness of a water-table aquifer. The thickness used in the calculations is limited to the proportion of the total sediment thickness in the saturated interval. The thicknesses defined for fine-grained interbeds should be the total thickness of the interbeds between the top and bottom of the model cell. For example, the total thickness for the upper aquifer shown in figure 1 would include the interbed thicknesses in the saturated and unsaturated zones.

Elastic Compaction of Aquifer Sediments

Storage changes resulting from elastic compression of aquifer sediments are based on the approach implemented in the storage (STO) package for MODFLOW 6 (Langevin and others, 2017), but have been modified to allow specific storage to be a function of effective stress and to separate water released from compression of aquifer and confining unit sediments from compression of water.

The storage contribution to the groundwater flow equation from elastic compaction of coarse-grained sediments is based on application of the storage term in equation 41. The expression for elastic compaction of coarse-grained sediments in cell n is

$$\Delta b_n^t = \frac{0.434 b_{e0_n}}{(1 + e_{0_n}) \bar{\sigma}_n'^t} C_{r_n} \left(\hat{\sigma}_n'^t - \hat{\sigma}_n'^{t_{old}} \right) \tag{59}$$

where b_{e0} is the initial thickness of elastic coarse-grained sediments in cell n (L). The thickness of elastic aquifer or confining unit sediments in cell n is calculated as

$$b_{e0_n} = f_{e0_n} \Delta v_n = f_{e0_n} \left(zt_n - zb_n \right), \tag{60}$$

where f_{e0} is the initial fraction of elastic coarse-grained sediments (measured vertically) in cell n (dimensionless). The fraction of coarse-grained sediments in a cell can change as a result of compaction of fine-grained sediments, unless the elastic- and inelastic-storage properties are identical for all sediments in a cell. If there are no interbeds in cell n, f_{e0} is set equal to 1. Substitution of equation 18 into equation 59 results in

$$\Delta b_n^t = \frac{0.434 b_{e0_n}}{(1 + e_{0_n}) \bar{\sigma}_n'^t} C_{r_n} \left[\left(\hat{\sigma}_n^t - h_n^t + zb_n \right) - \hat{\sigma}_n'^{t_{old}} \right], \tag{61}$$

which defines the general relation between compaction or expansion of sediments and the head at time t. Further simplification of equation 61 using equation 39 results in

$$\Delta b_n^t = b_{e0_n} \bar{S}_{ske_n}^t \left[\left(\hat{\sigma}_n^t - h_n^t + zb_n \right) - \hat{\sigma}_n'^{t_{old}} \right], \tag{62}$$

where $\bar{S}_{ske}$ is the average elastic skeletal specific storage value in cell n (dimensionless). The contribution of storage changes in cell n from elastic compression of coarse-grained sediments based on equations 42 and 62 is

$$Q_{sk_n}^t = \frac{A_n \Delta b_n^t}{t - t_{old}}, \tag{63}$$

where Q_{sk} is the flow from coarse-grained sediments in cell n ($L^3 T^{-1}$), taken as positive if water is released from storage (source of water).

Elastic and Inelastic Compaction of Fine-Grained Sediments

Fine-grained sediments that can undergo both elastic and inelastic compaction can be represented as interbeds that are assumed to be either in equilibrium or in disequilibrium with heads in surrounding coarse-grained sediments. In this report, the term "no-delay interbeds" is used to denote the interbeds for which the time for equilibration of interbed heads with surrounding aquifer heads is short compared to simulation time steps. The term "delay interbeds" is used to denote interbeds for which the time for equilibration of interbed heads and surrounding aquifer heads is significantly greater than the time steps used in the simulation. No-delay interbeds ignore the time delays owing to slow dissipation of head transients within the interbeds and assume that heads everywhere in the interbed equilibrate instantaneously with the head in the surrounding aquifer(s). Conversely for delay interbeds the process of slow dissipation of the heads in the interbed is explicitly represented in the model (Hoffmann and others, 2003). For relatively thick, extensive confining units, no-delay interbeds with the confining unit vertically divided into multiple cells can be applied to simulate the effects of delay in release of water from compressible interbeds (Hoffmann and others, 2003). The details of elastic and inelastic compaction of no-delay interbeds and delay interbeds are described below.

No-Delay Interbeds

The storage contribution to the groundwater flow equation from elastic and inelastic compaction of fine-grained sediments in no-delay interbeds is based on the application of the storage term in equation 40. The expression for elastic and inelastic compaction of no-delay interbed nb is

$$\Delta b_{nb}^t = \frac{0.434 b_{0_{nb}}}{\left(1 + e_{0_{nb}}\right) \bar{\sigma}_n'^t} \left[C_{c_{nb}}^t \left(\hat{\sigma}_n'^t - \hat{\sigma}_{c_n}'\right) + C_{r_{nb}} \left(\hat{\sigma}_{c_n}' - \hat{\sigma}_n'^{t_{old}}\right) \right], \tag{64}$$

where $\hat{\sigma}_c'$ is the preconsolidation stress in terms of the height of an equivalent column of water (L). Substitution of equation 18 into equation 64 results in

$$\Delta b_{nb}^t = \frac{0.434 b_{0_{nb}}}{\left(1 + e_{0_{nb}}\right) \bar{\sigma}_n'^t} \left[C_{c_{nb}}^t \left(\hat{\sigma}_n^t - h_n^t + zb_n - \hat{\sigma}_{c_n}'\right) + C_{r_{nb}} \left(\hat{\sigma}_{c_n}' - \hat{\sigma}_n'^{t_{old}}\right) \right] \tag{65}$$

and defines the general relation between compaction or expansion of sediments and the head at time t. Further simplification of equation 65 using equations 38 and 39 results in

$$\Delta b_{nb}^t = b_{0_{nb}} \left[\bar{S}_{sk_{nb}}^t \left(\hat{\sigma}_n^t - h_n^t + zb_n - \hat{\sigma}_{c_n}'\right) + \bar{S}_{ske_{nb}}^t \left(\hat{\sigma}_{c_n}' - \hat{\sigma}_n'^{t_{old}}\right) \right] \quad \bar{S}_{sk_{nb}}^t = \begin{cases} \bar{S}_{skv_{nb}}, & \hat{\sigma}_n'^t > \hat{\sigma}_{c_n}' \\ \bar{S}_{ske_{nb}}, & \hat{\sigma}_n'^t \le \hat{\sigma}_{c_n}' \end{cases}, \tag{66}$$

where $\bar{S}_{sk}$ is the appropriate average no-delay skeletal specific storage value in interbed nb at time t (dimensionless) and $\bar{S}_{skv}$ is the average inelastic no-delay skeletal specific storage value in interbed nb (dimensionless). The relation of $\hat{\sigma}'^t$ to $\hat{\sigma}_c'$ is used to determine whether the appropriate value of $\bar{S}_{sk}^t$ is $\bar{S}_{skv}$ or $\bar{S}_{ske}$. The contribution of storage changes in cell n from no-delay interbeds based on equations 42 and 66 is

$$Q_{ND_{nb}}^t = \frac{A_n \Delta b_{nb}^t}{t - t_{old}}, \tag{67}$$

where Q_{ND} is the flow from no-delay interbed nb and the cell n (L^3T^{-1}), taken as positive if water is released from storage in the no-delay interbed (source of water).
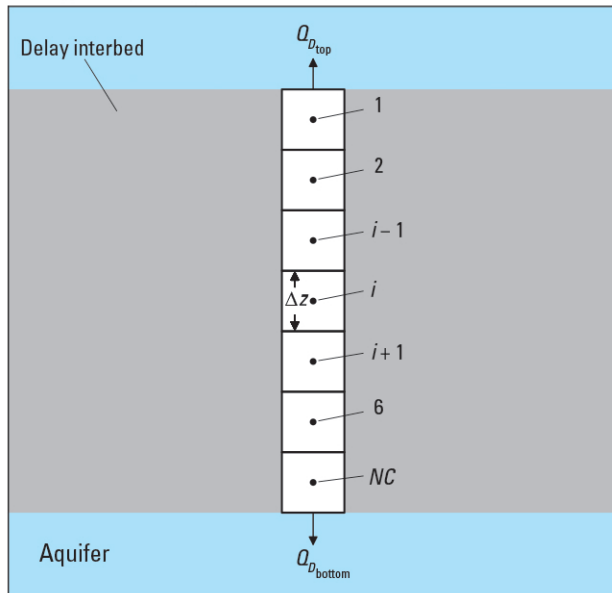
Delay Interbeds

When the horizontal extent of interbeds is much larger than the thickness, and the ratio of the average horizontal hydraulic conductivity of the aquifer and the vertical hydraulic conductivity of the interbed exceeds 10, flow in the interbed is vertical or nearly vertical. If the vertical hydraulic conductivity is constant, there are no internal sources or sinks, and flow is vertical the three-dimensional groundwater flow equation can be simplified to

$$K'_{zz}\frac{\partial^2 h}{\partial z^2} = S_s\frac{\partial h}{\partial t},$$ (68)

where K'_{zz} is the vertical hydraulic conductivity of the delay interbed (LT^{-1}). Matrix and water compressibility terms are included in the specific storage coefficient in equation 68 (see S_{sk} and S_{sw} in eq. 4). Because a delay interbed can be in disequilibrium with the head in a GWF cell, equation 68 is discretized using finite-differences as a one-dimensional column for each delay interbed as shown in figure 5A.
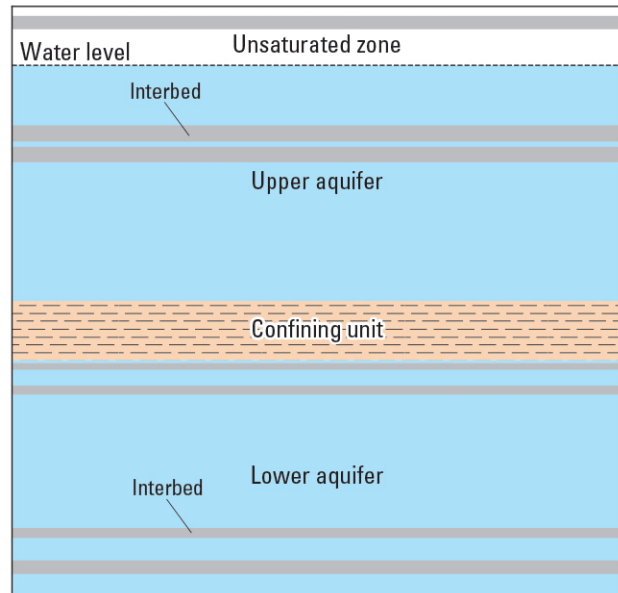
Figure 5. Diagram showing the the one-dimensional discretization of a delay interbed and its relation to interbeds in an aquifer. *A*, One-dimensional discretization of a delay interbed in an aquifer, where i is the delay bed cell number, NC is the number of nodes used to discretize the interbed, Δz is the spacing between nodes, $Q_{D_{top}}$ is the volumetric flow between the top of the delay interbed and the aquifer, and $Q_{D_{bottom}}$ is the volumetric flow between the bottom of the delay interbed and the aquifer; and *B*, aquifer system with two aquifers separated by a confining unit; the upper aquifer has three interbeds (one in the unsaturated zone) and the lower aquifer has four interbeds that are used to calculate the equivalent interbed properties (b_{equiv} and n_{equiv}) in each aquifer (see table 2) .

Stress calculations

The geostatic stress at the top of a one-dimensional delay interbed column is calculated assuming the bottom of the one-dimensional column is located at the bottom of cell n. The geostatic stress at the top of the delay interbed cell ($i = 1$) is calculated using

$$
\hat{\sigma}_{top_{nb}} = \begin{cases} \hat{\sigma}_n - (zt_{nb} - zb_n)\,G_{s_n} & \text{for } h_n \geq zt_n \\[2ex] \hat{\sigma}_n - \left[(zt_{nb} - \bar{h}_n)\,G_{m_n} + (\bar{h}_n - zb_n)\,G_{s_n}\right] & \text{for } h_n < zt_n \end{cases},
\tag{69}
$$

where $\hat{\sigma}_{top_{nb}}$ is the geostatic stress at the top of the one-dimensional delay interbed column representing delay interbed nb (L). The top of the one-dimensional delay interbed column (zt_{nb}), relative to the bottom of cell n, is calculated as $zt_{nb} = zb_n + b_{nb}$. The geostatic stress at the bottom of each delay interbed cell, based on equation 46, is calculated using

$$
\hat{\sigma}_i = \hat{\sigma}_{top_i} + b_{m_i} G_{m_n} + b_{s_i} G_{s_n},
\tag{70}
$$

where $\hat{\sigma}_{top_i}$ is the geostatic stress at the top of delay interbed cell i and is equal to $\hat{\sigma}_{top_{nb}}$ in delay interbed cell 1 or $\hat{\sigma}_{i-1}$ in all other delay interbed cells. The effective stress at the bottom of each delay interbed is calculated using

$$
\hat{\sigma}'_i = \hat{\sigma}_i - \bar{H}_i + zb_i,
\tag{71}
$$

where $\bar{H}$ is the linear corrected head in a delay interbed cell (L). $\bar{H}$ is calculated as

$$
\bar{H}_i = \begin{cases} H_i & \text{for } H_i \geq zb_i \\ zb_i & \text{for } H_i < zb_i \end{cases},
\tag{72}
$$

where H is the head in a delay interbed cell (L).

Like coarse-grained aquifer sediments and fine-grained sediments in no-delay interbeds, the inelastic and elastic skeletal specific storage coefficient for each delay interbed cell is calculated relative to the center of the saturated thickness of the cell ($\bar{z}_n$). Calculation of storage coefficients at the center of the saturated thickness of a cell requires adjustment of the effective stress results relative to the bottom of delay interbed cell i and cell n to the center of saturated thickness. The top and bottom of each interbed cell is adjusted to the center of the saturated thickness of cell n using

$$
\overline{zt}_i = \bar{z}_n + z_{offset_i} + \frac{\Delta z}{2} \quad \text{and}
\tag{73}
$$

$$
\overline{zb}_i = \bar{z}_n + z_{offset_i} - \frac{\Delta z}{2},
\tag{74}
$$

where $\overline{zt}$ is the top of delay interbed cell i relative to the center of the saturated thickness of cell n (L), z_{offset} is the offset of the center of delay interbed i from the center of the interbed, Δz is the thickness of each delay interbed cell (L), and $\overline{zt}$ is the bottom of delay interbed cell i relative to the center of the saturated thickness

of cell n (L). The center of the saturated thickness of a delay interbed adjusted to the center of the saturated thickness of cell n is

$$
\bar{z}_i = \begin{cases} \dfrac{1}{2}\left(\overline{zt}_i + \overline{zb}_i\right) & \text{for } H_i \geq zt_i \\[2ex] \dfrac{1}{2}\left(\bar{H}_i + \overline{zb}_i\right) & \text{for } H_i < zt_i \end{cases}.
\tag{75}
$$

The effective stress at the bottom of a delay interbed the cell is adjusted to the center of the saturated thickness in a delay interbed cell using

$$
\bar{\sigma}'_i = \hat{\sigma}'_i - \left(\bar{z}_i - zb_i\right)\left(G_{s_n} - 1\right)
\tag{76}
$$

and is used to calculate the inelastic and elastic skeletal specific storage coefficients for each delay interbed cell.

Delay interbed continuity equation

The continuity equation based on equation 68 (excluding the water) for each finite-difference cell in the one-dimensional column shown in figure 5B is

$$
Q^t_{DB_i} + Q^t_{STO_i} + Q^t_{WC_i} = 0,
\tag{77}
$$

where Q_{DB} is the volumetric flow rate from adjacent cells (L^3T^{-1}), Q_{STO} is the volumetric flow rate from storage in delay interbed cell i (L^3T^{-1}), and Q_{WC} is the volumetric storage change resulting from the compression of water in delay interbed cell i (L^3T^{-1}).

Delay interbed cell-to-cell flow

Q_{DB} for interior delay interbed cells ($1 < i < NC$) is the sum of the flow across the top and bottom faces of the cell and is calculated as

$$
Q^t_{DB_i} = Q^t_{DB_{i-1/2}} + Q^t_{DB_{i+1/2}}.
\tag{78}
$$

The volumetric flow across the top face of cell i, between delay interbed cells i and $i-1$, is

$$
Q^t_{DB_{i-1/2}} = K'_{zz} A \frac{H^t_{i-1} - H^t_i}{\Delta z},
\tag{79}
$$

where Δz is the thickness of each delay interbed cell (L). $Q_{DB_{i-1/2}}$ is taken as positive if water flows from delay interbed cell $i-1$ and i (source of water to cell i). Similarly the volumetric flow across the bottom face of cell i, between delay interbed cells i and $i+1$, is

$$
Q^t_{DB_{i+1/2}} = K'_{zz} A \frac{H^t_{i+1} - H^t_i}{\Delta z}.
\tag{80}
$$

$Q_{DB_{i+1/2}}$ is taken as positive if water flows from delay interbed cell $i+1$ and i (source of water to cell i).

For delay interbed cell 1 and NC, the volumetric flow between the delay bed and the GWF cell containing the interbed can be calculated directly using the vertical hydraulic conductivity of the interbed and the head difference between GWF cell n and the delay interbed cell. For the aquifer connection to the top of the interbed ($i = 1$), the volumetric flow between the delay interbed and the aquifer is

$$Q^t_{DB_{top}} = K'_{zz} A \frac{h^t_n - H^t_1}{\frac{\Delta z}{2}}, \tag{81}$$

which replaces the $Q^t_{DB_{i-1/2}}$ term in equation 78. Similarly, for the aquifer connection to the bottom of the interbed ($i = NC$), the volumetric flow between the delay interbed and the aquifer is

$$Q^t_{DB_{bottom}} = K'_{zz} A \frac{h^t_n - H^t_{NC}}{\frac{\Delta z}{2}}, \tag{82}$$

which replaces the $Q^t_{DB_{i+1/2}}$ term in equation 78.

Delay interbed cell compaction

The compaction in delay interbed cell i is

$$\Delta b^t_i = b_{0_i} \left[\bar{S}^t_{sk_i} \left(\hat{\sigma}^t_i - H^t_i + zb_i - \hat{\sigma}'_{c_i} \right) + \bar{S}^t_{ske_i} \left(\hat{\sigma}'_{c_i} - \hat{\sigma}'^{t_{old}}_i \right) \right], \tag{83}$$

where $\bar{S}_{sk}$ for delay interbed cell i is $\bar{S}_{skv}$ if $\hat{\sigma}' > \hat{\sigma}'_c$ or $\bar{S}_{ske}$ otherwise (see eq. 66 for $\hat{\sigma}'$ conditions). The volumetric flow rate from storage resulting from inelastic or elastic compaction in delay interbed cell i based on equations 42 and 83 is

$$Q^t_{STO_i} = \frac{A \Delta b^t_i}{t - t_{old}}. \tag{84}$$

Q_{STO} is taken as positive if water is released from storage in delay interbed cell i (source of water to cell i).

Delay interbed cell water compressibility

The volumetric flow rate from water compressibility in delay interbed cell i based on equation 42 is

$$Q^t_{WC_i} = \frac{A}{t - t_{old}} \left(S^{t_{old}}_{sw_i} b^{t_{old}}_i H^{t_{old}}_i - S^t_{sw_i} b^t_i H^t_i \right). \tag{85}$$

Q_{WC} is taken as positive if water is released by the expansion of water in delay interbed cell i (source of water to cell i). In order to simplify equation 85 for delay interbed cell i, the notation WC is introduced where

$$WC^{t_{old}}_i = A S^{t_{old}}_{sw_i} b^{t_{old}}_i \text{ and} \tag{86a}$$
$$WC^t_i = A S^t_{sw_i} b^t_i, \tag{86b}$$

where WC is the water compressibility coefficient (L^2). Using equation 86 to simplify equation 85 results in

$$Q_{WC_i}^t = \frac{WC_i^{t_{old}}}{t - t_{old}} H_i^{t_{old}} - \frac{WC_i^t}{t - t_{old}} H_i^t. \tag{87}$$

Delay Interbed Systems

As any aquifer might contain a large number of interbeds of different thicknesses, solving equation 68 for each interbed of fine-grained compressible sediments could easily become computationally prohibitive. Therefore to reduce the number of computations required, delay interbeds with the same vertical hydraulic conductivity, and elastic and inelastic skeletal specific storage within one GWF model cell can be grouped into a single delay interbed system. Helm (1975) determined the equivalent thickness for a system of individual delay interbeds with similar vertical hydraulic diffusivity can be computed as

$$b_{equiv_{nb}} = \sqrt{\frac{1}{N} \sum_{j=1}^{N} b_j^2}, \tag{88}$$

where b_{equiv} is the equivalent delay interbed thickness of delay interbed system nb (L), N is the number of interbeds with similar vertical hydraulic diffusivity in cell n grouped into delay interbed system nb, and b_j is the thickness of interbed j in cell n grouped into delay interbed system nb (L). To reproduce the total amount of interbed material and, thus, the correct compaction magnitude for the system of delay interbeds, the compaction and the volume of water exchanged with the surrounding aquifer needs to be multiplied by the factor

$$n_{equiv_{nb}} = \frac{\sum_{j=1}^{N} b_j}{b_{equiv}} \; . \tag{89}$$

By using equations 88 and 89, both the time history and the magnitude of the total compaction of the system of interbeds can be calculated. Thus, equation 68 is solved only once for a single equivalent interbed of thickness b_{equiv}, and the computed amounts of compaction and flow across the interbed boundaries are multiplied by n_{equiv}.

The total contribution of delay interbed system nb to storage changes in GWF cell n, based on equations 81 and 82, is

$$Q_{D_{nb}}^t = n_{equiv_{nb}} \frac{2K'_{zz_{nb}} A_n}{\Delta z_{nb}} \left(H_{NC_{nb}}^t + H_{1_{nb}}^t - 2h_n^t \right), \tag{90}$$

where Q_D is the flow between delay interbed system nb and cell n $(L^3 T^{-1})$, taken as positive if water is released from interbed storage into the aquifer (source of water to cell n).

Example System of Delay Interbed System Calculations

An example of a hypothetical aquifer system with an unconfined upper aquifer and confined aquifer separated by a confining unit (fig. 5B) is used to illustrate how the equivalent thickness and multiplier for a system of individual interbeds are calculated. The aquifer system is 100 meters thick, with a 50 meter thick upper aquifer, a 40 meter thick lower aquifer, and a 10 meter thick confining unit. The initial head is 10 meters below land surface throughout the aquifer system.

There are 3 interbeds in the upper aquifer that range from 2.25 to 2.76 meters in thickness (table 2) for a total interbed thickness of 7.62 meters (15.2 percent of the upper aquifer). Even though the upper aquifer is not fully saturated, the thickness of the interbed in the unsaturated zone should be included. There are 4 interbeds in the lower aquifer that range from 1.51 to 2.30 meters in thickness (table 2) for a total interbed thickness of 7.79 meters (19.4 percent of the lower aquifer).

Equation 88 is used to calculate the equivalent thickness of 2.55 and 1.98 meters for the upper and lower aquifers, respectively (table 2). The equivalent interbed multiplier, which is used to scale the volume of water exchanged between the equivalent interbed and the aquifer to the total delay interbed contribution to the aquifer, calculated using equation 89, is 2.99 for the upper aquifer and 3.94 for the lower aquifer (table 2).

Table 2.   Individual interbed thicknesses and computed equivalent interbed thicknesses and multipliers for delay interbeds in the upper and lower aquifers shown in figure 5B.

Interbed number	Interbed thickness (b_j), in meters	Equivalent interbed thickness (b_{equiv}), in meters	Equivalent interbed multiplier (n_{equiv}), unitless
Upper aquifer			
1	2.61		
2	2.25		
3	2.76		
	7.62	2.55	2.99
Lower aquifer			
1	1.51		
2	2.30		
3	1.69		
4	2.29		
	7.79	1.98	3.94

Water Compressibility

The contribution of water compressibility to storage changes in an aquifer based on equations 4 and 9 is

$$Q_{WC_n}^t = \frac{\Delta v_n S_{sw_n} A_n}{t - t_{old}} \left(h_n^{t_{old}} - h_n^t \right),$$ (91)

where Q_{WC} is the volumetric storage change resulting from the compression of water $(L^3 T^{-1})$. For a cell consisting of a combination of coarse-grained sediments and no-delay interbeds of fine-grained sediments equation 91 becomes

$$Q_{WC_n}^t = \frac{A_n}{t - t_{old}} \left(S_{sw_n}^{t_{old}} b_n^{t_{old}} h_n^{t_{old}} - S_{sw_n}^t b_n^t h_n^t \right),$$ (92)

where nd is the total number of delay interbeds.

Equation 92 uses the porosity at time t or t_{old} calculated using equation 21 and the thickness at time t or t_{old} calculated using equation 45. The product of the porosity and the thickness for a cell consisting of coarse-grained sediments and fine-grained sediments in no-delay interbeds is calculated as

$$\theta_n b_n = \theta_{e_n} b_{e_n} + \sum_{\substack{nb=1 \\ nb \in n}}^{nnd} \theta_{nb} b_{nb}, \tag{93}$$

where nnd is the total number of no-delay interbeds. In order to simplify equation 92 for coarse-grained sediments and no-delay interbeds in model cell n the notation WC defined in equation 86 is used where

$$WC_n^{t_{old}} = A_n S_{sw_n}^{t_{old}} b_n^{t_{old}}, \text{and} \tag{94a}$$

$$WC_n^t = A_n S_{sw_n}^t b_n^t. \tag{94b}$$

Using equation 94 to simplify equation 92 results in

$$Q_{WC_n}^t = \frac{WC_n^{t_{old}}}{t - t_{old}} h_n^{t_{old}} - \frac{WC_n^t}{t - t_{old}} h_n^t, \tag{95}$$

where Q_{WC} is positive if water is released by the expansion of water (source of water).

Incorporation of skeletal storage and interbed compaction into the CVFD Groundwater Flow Equation

To prepare the CVFD equation for solution using the standard formulation, it is convenient to rearrange the discretized groundwater flow equation for a cell so that all terms containing heads at the end of the current time step are grouped on the left-hand side of the equation, and all terms that are independent of the head at the end of the current time step are on the right-hand side. When the CSUB package is included, the resulting equation is

$$
\sum_{m \in \eta_n} C_{n,m}^t h_m^t + \left(- \sum_{m \in \eta_n} C_{n,m}^t + P_n^t - \frac{SC2_n^t + WC_n^t + A_n \sum \bar{S}_{sk_n}^t}{t - t_{old}} \right) h_n^t =
$$
$$
- Q_n^t - \left(\frac{SC2_n^{t_{old}} + WC_n^{t_{old}}}{t - t_{old}} \right) h_n^{t_{old}} - Q_n^{\star t},
$$
(96)

where $C_{n,m}$ is the conductance between connected cells n and m ($L^2 T^{-1}$), P_n is the sum of external-stress coefficients for cell n ($L^2 T^{-1}$), $SC2$ is a secondary storage capacity calculated by the STO Package using the specific yield and horizontal cell area for cell n (L^2), Q_n is a specified volumetric flux for cell n ($L^3 T^{-1}$), and $Q_n^\star$ is the sum of CSUB package terms for cell n that are calculated using $h^{t_{old}}$ or h^t from the previous iteration ($L^3 T^{-1}$). Because a backward-difference scheme is used in MODFLOW 6, the terms in equation 96 are for the end of the time step. Those terms in equation 96 that are a function of head (C_{nm} for unconfined conditions and Q_n and P_n for some stress packages, for example) are calculated using head from the previous iteration. $SC2$ is non-zero only when the head at time t or t_{old} is below the top of the cell (see Langevin and others, 2017).

The total contribution from storage to the groundwater flow equation (eq. 96) for cell n includes contributions from specific yield, water compressibility (eq. 95), elastic skeletal storage (eq. 63), and elastic- and inelastic-interbed skeletal storage (eqs. 67 and 90) and can be represented as

$$
Q_{TOTAL}^t = Q_{Sy_n}^t + Q_{WC_n}^t + Q_{sk_n}^t + \sum_{\substack{nb=1 \\ nb \in n}}^{nnd} Q_{ND_{nb}}^t + \sum_{\substack{nb=1 \\ nb \in n}}^{nd} Q_{D_{nb}}^t
$$
$$
= \left(\frac{SC2_n^{t_{old}} + WC_n^{t_{old}}}{t - t_{old}} \right) h_n^{t_{old}} - \left(\frac{SC2_n^t + WC_n^t + A_n \sum \bar{S}_{sk_n}^t}{t - t_{old}} \right) h_n^t + Q_n^{\star t},
$$
(97)

where Q_{TOTAL} is the total volumetric flow rate from storage in cell n ($L^3 T^{-1}$), Q_{Sy} is the volumetric flow rate from specific yield in cell n ($L^3 T^{-1}$), and nd is the total number of delay interbeds.

The entire system of equations, which includes a groundwater flow equation (eq. 96) for each variable and constant-head cell in the grid, can be written in matrix form as

$$
\mathbf{A}\mathbf{x} = \mathbf{r},
$$
(98)

where $\mathbf{A}$ is a coefficient matrix, $\mathbf{x}$ is a vector of unknown heads, and $\mathbf{r}$ is a vector containing known components of the groundwater flow equation. Assembly of the coefficient matrix $\mathbf{A}$ and the vector $\mathbf{r}$ occurs through a series of subroutine and method calls by the MODFLOW 6 program.

The storage terms in equation 97, except for Q_{Sy_n}, are added to the system of equations by the CSUB package. The compressible storage terms in equation 97 are a nonlinear function of the current effective stress (see eqs. 38 and 39). These nonlinearities are resolved through iteration by repeatedly formulating and solving equation 98 using $\mathbf{A}$ matrix and $\mathbf{r}$ vector entries recalculated using heads from the previous iteration and are referred to as outer iterations.

The assembled $\mathbf{A}$ matrix and $\mathbf{r}$ vector for an outer iteration are then transferred to the linear solver, which solves equation 98 for the $\mathbf{x}$ vector. Outer iterations are continued until the specified head and flow convergence criteria are met. If delay interbeds are simulated, outer iterations are also continued until the ratio of $Q_{STO} + Q_{WC} - Q_D$ and A_n for a delay interbed meet the specified head convergence criteria for every delay interbed. Refer to Langevin and others (2017) and Hughes and others (2017) for additional information on how other groundwater flow equation terms are formulated in MODFLOW 6 and how the assembled system of equations is solved, respectively. CSUB package storage terms that are added to the diagonal of the $\mathbf{A}$ matrix and the $\mathbf{r}$ vector for each outer iteration are presented below.

Standard Formulation

The standard formulation available in MODFLOW 6 can be applied when cells representing aquifers and confining units do not completely dewater during the simulation. Although equations 38 and 39 are nonlinear, the nonlinearity may be mild enough to allow for the use of the standard formulation to assemble CSUB package terms.

Elastic compaction of coarse-grained sediments

For the case where the head in cell n is above the bottom of the cell for the previous time step (t_{old}) or the current iteration (k), the contribution of elastic compression of coarse-grained sediments to the groundwater flow equations based on equation 63 is defined as

$$
Q_{sk_n}^k = \frac{A_n b_{e0_n} \bar{S}_{ske_n}^{k-1}}{t - t_{old}} \left[S_{F_n}^{k-1} \left(\hat{\sigma}_n^{k-1} - h_n^k + zb_n \right) - \check{S}_{F_n} \hat{\sigma}_n'^{\,t_{old}} \right] +
$$
$$
\frac{A_n b_{e0_n} \bar{S}_{ske_n}^{k-1}}{t - t_{old}} S_{F_n}^{k-1} \left(h_n^{k-1} - \bar{h}_n^{k-1} \right), \tag{99}
$$

where S_F is the linear saturated cell fraction based on the current (h_n^{k-1}) head and $\check{S}_{F_n}$ is the linear saturated cell fraction based on the current (h_n^{k-1}) or previous ($h_n^{t_{old}}$) head. The second term on the right-hand side of equation 99 is a flow correction term that corrects Q_{sk} when h_n is less than zb_n. In the case where h_n is greater than zb_n, the flow correction term is equal to zero. The linear cell saturation fraction function is introduced to generalize equation 63 for unconfined (water-table) conditions and is calculated as

$$
S_{F_n} = \begin{cases} 1 & \text{for } h_n \geq zt_n \\[2mm] \dfrac{h_n - zb_n}{zt_n - zb_n} & \text{for } zb_n \leq h_n < zt_n \\[2mm] 0 & \text{for } h < zb. \end{cases} \tag{100}
$$

S_{F_n} is one for all values of h if cell n is defined to be fully saturated (nonconvertible) in the MODFLOW 6 storage package (see "Confined and Convertible Cells" section in chapter 4 of Langevin and others, 2017).

The head transition function is used to correct the head when the interbed cell is dry and the effective stress is equal to the geostatic stress.

Use of $\check{S}_{F_n}$ calculated with the previous head is consistent with the formulation used in the standard storage (STO) package. The use of $\check{S}_{F_n}$ calculated with the current head is consistent with the formulation used in the MODFLOW-2005 SUB-WT subsidence package (Leake and Galloway, 2007).

Rearranging equation 99 to move terms dependent on the current value of h to the left-hand side of the groundwater flow equation and all other terms to the right-hand side of the groundwater flow equation results in

$$
-S_{F_n}^{k-1} \frac{A_n b_{e0_n} \bar{S}_{ske_n}^{k-1}}{t - t_{old}} h_n^k = -\frac{A_n b_{e0_n} \bar{S}_{ske_n}^{k-1}}{t - t_{old}} \left[S_{F_n}^{k-1} \left(\hat{\sigma}_n^{k-1} + z b_n \right) - \check{S}_{F_n} \hat{\sigma}_n'^{t_{old}} \right] - \frac{A_n b_{e0_n} \bar{S}_{ske_n}^{k-1}}{t - t_{old}} S_{F_n}^{k-1} \left(h_n^{k-1} - \bar{h}_n^{k-1} \right),
$$
(101)

No-delay interbed compaction

For the case where the head in cell n is above the bottom of the cell for the previous time step (t_{old}) or the current iteration (k), the contribution of a no-delay interbed nb in cell n to the groundwater flow equation based on equation 67 is defined as

$$
Q_{ND_{nb}}^k = \frac{A_n b_{0_{nb}}}{t - t_{old}} \left[S_{F_n}^{k-1} \bar{S}_{sk_{nb}}^{k-1} \left(\hat{\sigma}_n^{k-1} - h_n^k + z b_n - \hat{\sigma}_{c_n}' \right) + \check{S}_{F_n} \bar{S}_{ske_{nb}}^{k-1} \left(\hat{\sigma}_{c_n}' - \hat{\sigma}_n'^{t_{old}} \right) \right] + \frac{A_n b_{0_{nb}}}{t - t_{old}} S_{F_n}^{k-1} \bar{S}_{sk_{nb}}^{k-1} \left(h_n^{k-1} - \bar{h}_n^{k-1} \right).
$$
(102)

The saturated cell fraction for cell n is introduced to generalize equation 67 for water-table conditions. S_{F_n} is one for all values of h if cell n is defined to be nonconvertible (confined) in the MODFLOW 6 storage package. The second term on the right-hand side of equation 102 is a flow correction term that corrects Q_{ND} when h_n is less than $z b_n$. Rearranging equation 102 to move terms dependent on the current value of h to the left-hand side of the groundwater flow equation and all other terms to the right-hand side of the groundwater flow equation results in

$$
-\frac{\bar{S}_{sk_{nb}}^{k-1} A_n b_{0_{nb}}}{t - t_{old}} S_{F_n}^{k-1} h_n^k = -\frac{A_n b_{0_{nb}}}{t - t_{old}} \left[S_{F_n}^{k-1} \bar{S}_{sk_{nb}}^{k-1} \left(\hat{\sigma}_n^{k-1} + z b_n - \hat{\sigma}_{c_n}' \right) + \check{S}_{F_n} \bar{S}_{ske_{nb}}^{k-1} \left(\hat{\sigma}_{c_n}' - \hat{\sigma}_n'^{t_{old}} \right) \right] - \frac{A_n b_{0_{nb}}}{t - t_{old}} S_{F_n}^{k-1} \bar{S}_{sk_{nb}}^{k-1} \left(h_n^{k-1} - \bar{h}_n^{k-1} \right).
$$
(103)

Delay interbed system compaction

For the current iteration (k), the contribution of a delay interbed system nb in cell n to the groundwater flow equation based on equation 90 is defined as

$$
Q_{D_{nb}}^k = n_{equiv_{nb}} \frac{2 K_{zz_{nb}}' A_n}{\Delta z_{nb}} \left(H_{NC_{nb}}^{k-1} + H_{1_{nb}}^{k-1} - 2 h_n^k \right).
$$
(104)

Rearranging equation 104 to move terms dependent on the current value of h to the left-hand side of the groundwater flow equation and all other terms to the right-hand side of the groundwater flow equation results in

$$-n_{equiv_{nb}} \frac{4K'_{zz_{nb}} A_n}{\Delta z_{nb}} h_n^k = -n_{equiv_{nb}} \frac{2K'_{zz_{nb}} A_n}{\Delta z_{nb}} \left(H_{NC_{nb}}^{k-1} + H_{1_{nb}}^{k-1} \right). \tag{105}$$

Water Compressibility

For the case where the head in cell n is above the bottom of the cell for the previous time step (t_{old}) and the current iteration (k), the contribution of water compressibility to the groundwater flow equation based on equation 95 is defined as

$$Q_{WC_n}^k = \frac{WC_n^{t_{old}}}{t - t_{old}} \check{S}_{F_n} h_n^{t_{old}} - \frac{WC_n^{k-1}}{t - t_{old}} S_{F_n}^{k-1} h_n^k. \tag{106}$$

The saturated cell fraction for cell n is introduced to generalize equation 95 for water-table conditions. S_{F_n} is one if cell n is defined to be nonconvertible (confined) in the MODFLOW 6 storage package. Rearranging equation 106 to move terms dependent on the current value of h to the left-hand side of the groundwater flow equation and all other terms to the right-hand side of the groundwater flow equation results in

$$-\frac{WC_n^{k-1}}{t - t_{old}} S_{F_n}^{k-1} h_n^k = -\frac{WC_n^{t_{old}}}{t - t_{old}} \check{S}_{F_n} h_n^{t_{old}}. \tag{107}$$

Newton-Raphson Formulation

The CSUB package of MODFLOW 6 (Langevin and others, 2017) includes a Newton-Raphson formulation option that can improve model convergence for highly nonlinear problems. When the Newton-Raphson formulation is used, discontinuous derivatives can cause nonconvergence in the neighborhood of the discontinuity (Kavetski and Kuczera, 2007). The linear cell saturation is a function of head and the derivative of equation 100 is

$$\frac{\partial S_F}{\partial h} = \begin{cases} 0 & \text{for } h \geq zt \\ \dfrac{1}{zt - zb} & \text{for } zb \leq h < zt \\ 0 & \text{for } h < zb \end{cases}, \tag{108}$$

which is discontinuous in the neighborhood of zb and zt. The linear head correction ($\bar{h}$) is also a function of head and the derivative of equation 51 is

$$\frac{\partial \bar{h}}{\partial h} = \begin{cases} 1 & \text{for } h \geq zb \\ 0 & \text{for } h < zb \end{cases}, \tag{109}$$

which is discontinuous in the neighborhood of zb.

The geostatic stress, pore pressure, and effective stress are a function of the head in a cell. The derivative of equation 55 is

$$\frac{\partial \hat{\sigma}'}{\partial h} = \begin{cases} 0 & \text{for } h < zb \\ G_s - G_m - 1 & \text{for } zb \leq h < zt \, , \\ -1 & \text{for } h \geq zt \end{cases} \tag{110}$$

which is discontinuous in the neighborhood of zb and zt. Like the effective stress at the bottom of a cell, the average effective stress in a cell is a function of head. The derivative of equation 58 is

$$\frac{\partial \bar{\sigma}'}{\partial h} = \begin{cases} \dfrac{\partial \hat{\sigma}'}{\partial h} & \text{for } h < zb \\ \dfrac{\partial \hat{\sigma}'}{\partial h} - \dfrac{1}{2}(G_s - 1) = \dfrac{1}{2}G_s - G_m - \dfrac{1}{2} & \text{for } zb \leq h < zt \, , \\ -1 & \text{for } h \geq zt \end{cases} \tag{111}$$

which is discontinuous in the neighborhood of zb and zt.

Applying the chain rule to equation 38, with $g(x) = \bar{\sigma}'$ and $g'(x) =$ equation 111, the derivative of the inelastic skeletal specific storage value, with effective stress in terms of the height of water, is

$$\frac{\partial \bar{S}_{skv}}{\partial h} = \begin{cases} 0 & \text{for } h < zb \\ -\dfrac{0.434 C_c}{(1 + e_0)(\bar{\sigma}')^2}\left(\dfrac{1}{2}G_s - G_m - \dfrac{1}{2}\right) & \text{for } zb \leq h < zt \, . \\ \dfrac{0.434 C_c}{(1 + e_0)(\bar{\sigma}')^2} & \text{for } h \geq zt \end{cases} \tag{112}$$

Because the effective stress in equation 112 is squared, the derivative of the inelastic skeletal specific storage value is small relative to the derivative of the linear saturation function (eq. 108) and the linear head correction (eq. 109). For example, for a 10-meter cell with $C_c = 0.25$, $e_0 = 0.33$, $G_s = 2$, and $G_m = 1.7$, the maximum derivative of the inelastic skeletal specific storage value, the linear saturation function, and the linear head correction are 3.4×10^{-4}, 0.1, and 1, respectively. The derivative of the elastic skeletal specific storage value would be one or two orders of magnitude less than the derivative of the inelastic skeletal specific storage value. For larger cells or cells located at depth, the derivative of the inelastic skeletal specific storage value would be even smaller than the derivative of the linear saturation function; for example, the derivatives of the inelastic skeletal specific storage value, the linear saturation function, and the linear head correction for a 10-meter cell located below 100 meters of saturated sediments are 1.4×10^{-5}, 0.1, and 1, respectively. As a result, the inelastic and elastic skeletal specific-storage values are assumed to be independent of the head when solving the linear equations within a nonlinear iteration loop, which simplifies the analytical derivatives of the compaction equations.

Quadratic smoothing (Niswonger and others, 2011) is applied to the linear saturated fraction (eq. 100) that is used in equations 101, 103, 104, and 107. The quadratically smoothed saturated fraction is calculated using

$$S_F^* = \begin{cases} 0 & \text{for } h < zb \\ \dfrac{A_\Omega}{2\Omega}\left(\dfrac{h - zb}{zt - zb}\right)^2 & \text{for } zb \le h < zb + \Omega \\ A_\Omega \dfrac{h - zb}{zt - zb} + \dfrac{1}{2}(1 - A_\Omega) & \text{for } zb + \Omega \le h < zt - \Omega \,, \\ 1 - \dfrac{A_\Omega}{2\Omega}\left(1 - \dfrac{h - zb}{zt - zb}\right)^2 & \text{for } zt - \Omega \le h < z \\ 1 & \text{for } h \ge zt \end{cases} \tag{113}$$

where S_F^* is the quadratically smoothed saturation function (dimensionless), Ω is a small distance over which quadratic smoothing occurs (L), and A_Ω is defined as $A_\Omega = \frac{1}{1-\Omega}$ (L^{-1}). In MODFLOW 6, Ω is fixed at 1×10^{-6}, which is equal to the Ω used in other packages. As indicated by equation 113, the saturated fraction will be 0 and 1 for convertible cells in which the head is below the bottom and above the top elevation of a cell, respectively, as shown in figure 6. For confined cells, the saturated fraction is always 1. The derivative of equation 113 is

$$\frac{\partial S_F^*}{\partial h} = \begin{cases} 0 & \text{for } h < zb \\ \dfrac{A_\Omega}{\Omega (zt - zb)} \dfrac{h - zb}{zt - zb} & \text{for } zb \le h < zb + \Omega \\ \dfrac{A_\Omega}{(zt - zb)} & \text{for } zb + \Omega \le h < zt - \Omega \,, \\ \dfrac{A_\Omega}{\Omega (zt - zb)}\left(1 - \dfrac{h - zb}{zt - zb}\right) & \text{for } zt - \Omega \le h < zt \\ 0 & \text{for } h \ge zt \end{cases} \tag{114}$$

which is shown in figure 6B.

Quadratic smoothing (Panday and others, 2013) is also applied to the linear head correction (eq. 51) that is used in equations 101, 103, and 104. The quadratically smoothed head correction is calculated using

$$\bar{h}^\star = \begin{cases} zb & \text{for } h - zb < -\epsilon \\ \dfrac{(h - zb)^2}{4\epsilon} + \dfrac{(h - zb)}{2} + \dfrac{\epsilon}{4} + zb & \text{for } -\epsilon < h - zb < +\epsilon \,, \\ h & \text{for } h - zb \ge +\epsilon \end{cases} \tag{115}$$

where ϵ is the interval over which the head transition function is smoothed. In MODFLOW 6, ϵ is fixed at 5×10^{-7}, which is half of the quadratic smoothing distance (Ω) used in the quadratically smoothed cell saturations (eq. 113). The relation of $\bar{h}^\star$ to h over smoothing interval ϵ is shown in figure 7A. The unsmoothed
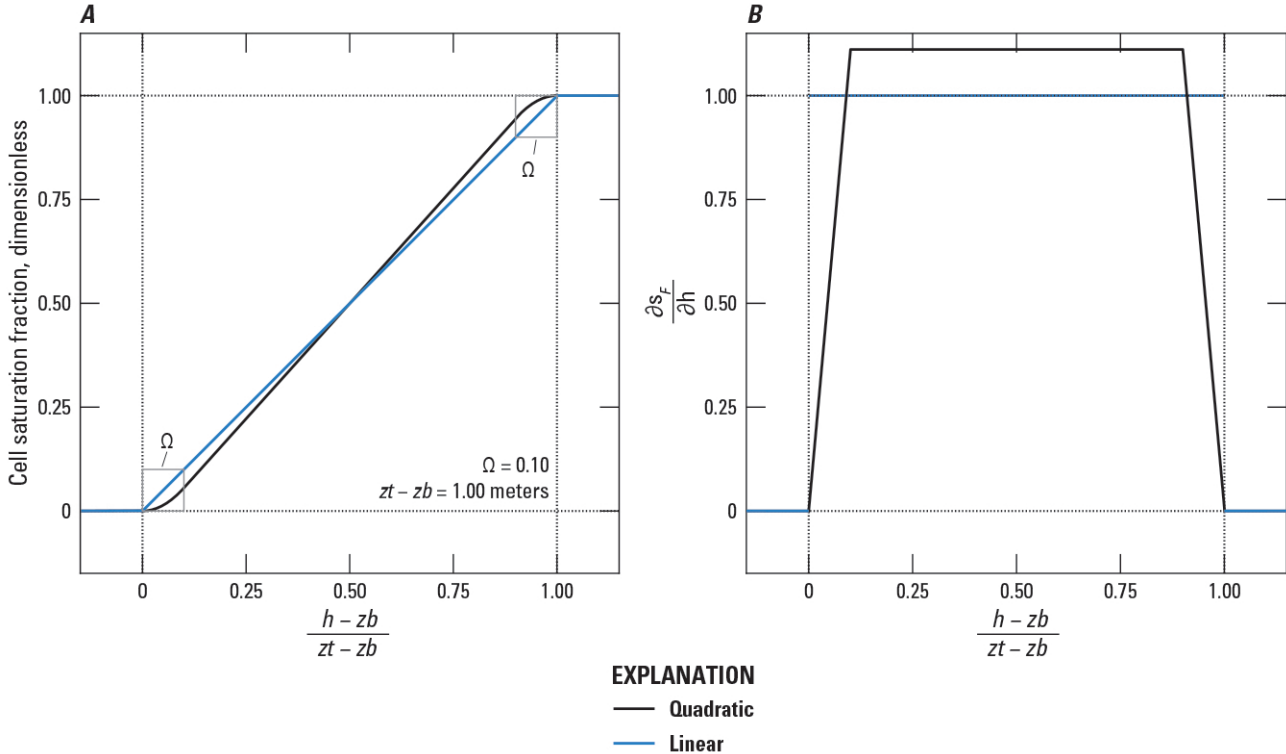
Figure 6.   Graphs showing cell saturation fraction functions and the derivatives of cell saturation fraction functions. *A*, quadratic and linear cell saturation fraction functions and *B*, derivatives of the quadratic and linear cell saturation functions. Figure 6*A* modified from Niswonger and others, 2011.

(linear) head transition function is also shown in figure 7*A*. The derivative of $\bar{h}^{\star}$ with respect to the head in cell n is

$$\frac{\partial \bar{h}^{\star}}{\partial h} = \begin{cases} 0 & \text{for } h - zb < -\epsilon \\ \dfrac{h - zb}{2\epsilon} + \dfrac{1}{2} & \text{for } -\epsilon < h - zb < +\epsilon \ . \\ 1 & \text{for } h - zb \geq +\epsilon \end{cases} \tag{116}$$

The relation of $\frac{\partial \bar{h}^{\star}}{\partial h}$ to h over smoothing interval ϵ is shown in figure 7*B*. The derivative of the unsmoothed (linear) head transition function is also shown in figure 7*B* and shows the discontinuity that occurs when the head is at the bottom of the delay interbed cell i.

Elastic compaction of aquifer sediments

Simplification of equation 99 removes the current head value (h^{k-1}) and results in

$$Q_{sk_n}^{k} = \frac{A_n b_{e0_n} \bar{S}_{ske_n}^{k-1}}{t - t_{old}} \left[S_{F_n}^{*\,k-1} \left(\hat{\sigma}_n^{k-1} - \bar{h}_n^{*\,k-1} + zb_n \right) - \check{S}_{F_n}^{\star} \hat{\sigma}_n'^{\,t_{old}} \right]. \tag{117}$$

The derivative of equation 117 with respect to h_n, assuming $\bar{S}_{ske}$ is head-independent and $\check{S}_{F_n}$ is calculated using the previous head, is
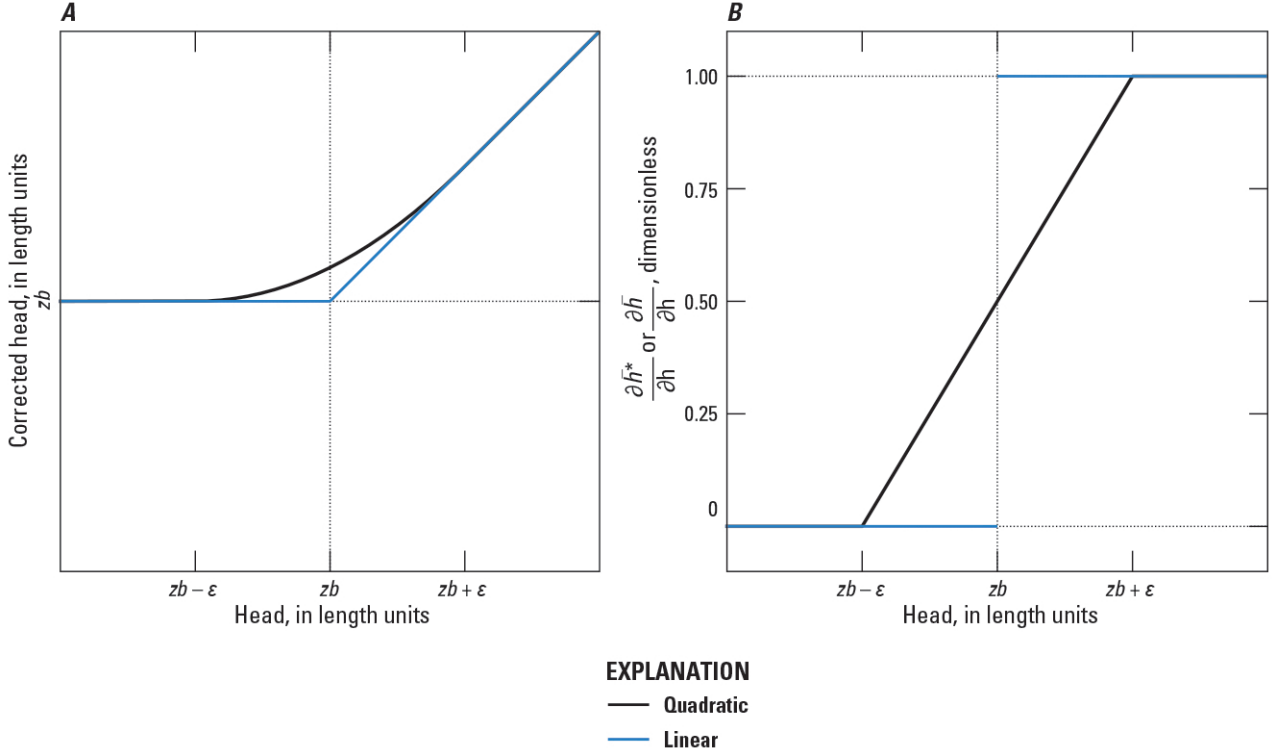
Figure 7. Graphs showing head correction functions and the derivatives of head correction functions. *A*, quadratically smoothed and linear head correction functions; and *B*, derivatives of the quadratically smoothed and linear head correction functions. $\partial \bar{h}^{\star}/\partial h$ and $\partial \bar{h}/\partial h$ are the derivatives of the quadratically smoothed and linear head correction functions, respectively. Figure 7*A* modified from Panday and others, 2013.

$$\frac{\partial Q_{sk_n}^{k-1}}{\partial h_n} = -\frac{\bar{S}_{ske_n}^{k-1} A_n b_{e0_n}}{t - t_{old}} S_{F_n}^{*\,k-1} \frac{\partial \bar{h}_n^{*\,k-1}}{\partial h_n} + \frac{\bar{S}_{ske_n}^{k-1} A_n b_{e0_n}}{t - t_{old}} \left(\hat{\sigma}_n^{k-1} - \bar{h}_n^{*\,k-1} + zb_n \right) \frac{\partial S_{F_n}^{*\,k-1}}{\partial h_n}. \tag{118}$$

The fully implicit form of the Newton-Raphson formulation for the contribution of coarse-grained sediments in cell n in the form of equation 2-30 in Langevin and others (2017) is

$$\frac{\partial Q_{sk_n}^{k-1}}{\partial h_n} h_n^k = -Q_{sk_n}^{k-1} + \frac{\partial Q_{sk_n}^{k-1}}{\partial h_n} h_n^{k-1}. \tag{119}$$

Substitution of equations 117 and 118 into equation 119 results in

$$\left[-\frac{\bar{S}_{ske_n}^{k-1} A_n b_{e0_n}}{t - t_{old}} S_{F_n}^{*\,k-1} \frac{\partial \bar{h}_n^{*\,k-1}}{\partial h_n} + \frac{\bar{S}_{ske_n}^{k-1} A_n b_{e0_n}}{t - t_{old}} \left(\hat{\sigma}_n^{k-1} - \bar{h}_n^{*\,k-1} + zb_n \right) \frac{\partial S_{F_n}^{*\,k-1}}{\partial h_n} \right] h_n^k =$$
$$-\frac{\bar{S}_{sk_n}^{k-1} A_n b_{e0_n}}{t - t_{old}} \left[S_{F_n}^{*\,k-1} \left(\hat{\sigma}_n^{k-1} - \bar{h}_n^{*\,k-1} + zb_n \right) - \check{S}_{F_n}^{\star} \hat{\sigma}_n'^{\,t_{old}} \right] \tag{120}$$
$$+ \left[-\frac{\bar{S}_{ske_n}^{k-1} A_n b_{e0_n}}{t - t_{old}} S_{F_n}^{*\,k-1} \frac{\partial \bar{h}_n^{*\,k-1}}{\partial h_n} + \frac{\bar{S}_{ske_n}^{k-1} A_n b_{e0_n}}{t - t_{old}} \left(\hat{\sigma}_n^{k-1} - \bar{h}_n^{*\,k-1} + zb_n \right) \frac{\partial S_{F_n}^{*\,k-1}}{\partial h_n} \right] h_n^{k-1}.$$

To complete the Newton-Raphson formulation, the terms added to the left and right-hand sides during the standard formulation step (eq. 101) are modified by adding

$$\frac{\bar{S}_{ske_n}^{k-1} A_n b_{e0_n}}{t - t_{old}} S_{F_n}^{*\,k-1} \left(1 - \frac{\partial \bar{h}_n^{*\,k-1}}{\partial h_n}\right) + \frac{\bar{S}_{ske_n}^{k-1} A_n b_{e0_n}}{t - t_{old}} \left(\hat{\sigma}_n^{k-1} - \bar{h}_n^{*\,k-1} + zb_n\right) \frac{\partial S_{F_n}^{*\,k-1}}{\partial h_n} \tag{121}$$

to the left-hand side and

$$\left[\frac{\bar{S}_{ske_n}^{k-1} A_n b_{e0_n}}{t - t_{old}} S_{F_n}^{*\,k-1} \left(1 - \frac{\partial \bar{h}_n^{*\,k-1}}{\partial h_n}\right) + \frac{\bar{S}_{ske_n}^{k-1} A_n b_{e0_n}}{t - t_{old}} \left(\hat{\sigma}_n^{k-1} - \bar{h}_n^{*\,k-1} + zb_n\right) \frac{\partial S_{F_n}^{*\,k-1}}{\partial h_n}\right] h^{k-1} \tag{122}$$

to the right-hand side. The term $\left(1 - \frac{\partial \bar{h}_n^{*\,k-1}}{\partial h_n}\right)$ in equation 121 removes the $-\frac{\bar{S}_{ske_n}^{k-1} A_n b_{e0_n}}{t - t_{old}} S_{F_n}^{*\,k-1}$ term added to the left-hand side during the standard formulation step. Similarly, the term $\left(1 - \frac{\partial \bar{h}_n^{*\,k-1}}{\partial h_n}\right)$ in equation 122 removes the portion of the correction term calculated with the current head value that was added to the right-hand side during the standard formulation step.

In cases where $\check{S}_{F_n}$ in equation 117 is calculated using the current head, $\hat{\sigma}_n'^{\,t_{old}}$ is subtracted from the terms in the parentheses of the second term on the right-hand side of equation 118. In this case, all instances of $\left(\hat{\sigma}_n^{k-1} - \bar{h}_n^{k-1} + zb_n\right)$ in equations 121 and 122 would be replaced by $\left(\hat{\sigma}_n^{k-1} - \bar{h}_n^{k-1} + zb_n - \hat{\sigma}_n'^{\,t_{old}}\right)$.

No-delay interbed compaction

Simplification of equation 102 removes the current head value (h^{k-1}) and results in

$$Q_{ND_{nb}}^k = \frac{A_n b_{0_{nb}}}{t - t_{old}} \left[S_{F_n}^{*\,k-1} \bar{S}_{sk_{nb}}^{k-1} \left(\hat{\sigma}_n^{k-1} - \bar{h}_n^k + zb_n - \hat{\sigma}_{c_n}'\right) + \check{S}_{F_n}^\star \bar{S}_{ske_{nb}}^{k-1} \left(\hat{\sigma}_{c_n}' - \hat{\sigma}_n'^{\,t_{old}}\right)\right]. \tag{123}$$

The derivative of equation 123 with respect to h_n, assuming $\bar{S}_{sk_{nb}}$ and $\bar{S}_{ske_{nb}}$ are head-independent and $\check{S}_{F_n}^\star$ is calculated using the previous head, is

$$\frac{\partial Q_{ND_{nb}}^{k-1}}{\partial h_n} = -\frac{\bar{S}_{sk_{nb}}^{k-1} A_n b_{0_{nb}}}{t - t_{old}} S_{F_n}^{*\,k-1} \frac{\partial \bar{h}_n^{*\,k-1}}{\partial h_n} + \frac{\bar{S}_{sk_{nb}}^{k-1} A_n b_{0_{nb}}}{t - t_{old}} \left(\hat{\sigma}_n^{k-1} - \bar{h}_n^{k-1} + zb_n - \hat{\sigma}_{c_n}'\right) \frac{\partial S_{F_n}^{*\,k-1}}{\partial h_n}. \tag{124}$$

The fully implicit form of the Newton-Raphson formulation for the contribution of no-delay interbed nb to cell n in the form of equation 2-30 in Langevin and others (2017) is

$$\frac{\partial Q_{ND_{nb}}^{k-1}}{\partial h_n} h_n^k = -Q_{ND_{nb}}^{k-1} + \frac{\partial Q_{ND_{nb}}^{k-1}}{\partial h_n} h_n^{k-1}. \tag{125}$$

Substitution of equations 123 and 124 into equation 125 results in

$$\left[-\frac{\bar{S}_{sk_{nb}}^{k-1}A_n b_{0_{nb}}}{t-t_{old}}S_{F_n}^{*\,k-1}\frac{\partial\bar{h}_n^{*\,k-1}}{\partial h_n}+\frac{\bar{S}_{sk_{nb}}^{k-1}A_n b_{0_{nb}}}{t-t_{old}}\left(\hat{\sigma}_n^{k-1}-\bar{h}_n^{k-1}+zb_n-\hat{\sigma}_{c_n}'\right)\frac{\partial S_{F_n}^{*\,k-1}}{\partial h_n}\right]h_n^k=$$
$$-\frac{A_n b_{0_n}}{t-t_{old}}\left[S_{F_n}^{*\,k-1}\bar{S}_{sk_{nb}}^{k-1}\left(\sigma_n^{k-1}-\bar{h}_n^{k-1}+zb_n-\hat{\sigma}_{c_n}'\right)-\check{S}_{F_n}^{\star}\bar{S}_{ske_{nb}}^{k-1}\left(\hat{\sigma}_{c_n}'-\hat{\sigma}_n'^{\,t_{old}}\right)\right] \quad (126)$$
$$+\left[-\frac{\bar{S}_{sk_n}^{k-1}A_n b_{0_n}}{t-t_{old}}S_{F_n}^{*\,k-1}\frac{\partial\bar{h}_n^{*\,k-1}}{\partial h_n}+\frac{\bar{S}_{sk_{nb}}^{k-1}A_n b_{0_{nb}}}{t-t_{old}}\left(\hat{\sigma}_n^{k-1}-\bar{h}_n^{k-1}+zb_n-\hat{\sigma}_{c_n}'\right)\frac{\partial S_{F_n}^{*\,k-1}}{\partial h_n}\right]h_n^{k-1}.$$

To complete the Newton-Raphson formulation, the terms added to the left and right-hand sides during the standard formulation step (eq. 103) are modified by adding

$$\frac{\bar{S}_{sk_{nb}}^{k-1}A_n b_{0_{nb}}}{t-t_{old}}S_{F_n}^{*\,k-1}\left(1-\frac{\partial\bar{h}_n^{*\,k-1}}{\partial h_n}\right)+\frac{\bar{S}_{sk_{nb}}^{k-1}A_n b_{0_{nb}}}{t-t_{old}}\left(\hat{\sigma}_n^{k-1}-\bar{h}_n^{k-1}+zb_n-\hat{\sigma}_{c_n}'\right)\frac{\partial S_{F_n}^{*\,k-1}}{\partial h_n} \quad (127)$$

to the left-hand side and

$$\left[\frac{\bar{S}_{sk_{nb}}^{k-1}A_n b_{0_{nb}}}{t-t_{old}}S_{F_n}^{*\,k-1}\left(1-\frac{\partial\bar{h}_n^{*\,k-1}}{\partial h_n}\right)+\frac{\bar{S}_{sk_{nb}}^{k-1}A_n b_{0_{nb}}}{t-t_{old}}\left(\hat{\sigma}_n^{k-1}-\bar{h}_n^{k-1}+zb_n-\hat{\sigma}_{c_n}'\right)\frac{\partial S_{F_n}^{*\,k-1}}{\partial h_n}\right]h_n^{k-1} \quad (128)$$

to the right-hand side. The term $\left(1-\frac{\partial\bar{h}_n^{*\,k-1}}{\partial h_n}\right)$ in the first term of equation 127 removes the

$-\frac{\bar{S}_{sk_{nb}}^{k-1}A_n b_{0_{nb}}}{t-t_{old}}S_{F_n}^{*\,k-1}$ term added to the left-hand side during the standard formulation step. Similarly, the term $\left(1-\frac{\partial\bar{h}_n^{*\,k-1}}{\partial h_n}\right)$ in the first term of equation 128 removes the portion of the correction term calculated with the current head value that was added to the right-hand side during the standard formulation step.

In cases where $\check{S}_{F_n}^{\star}$ in equation 123 is calculated using the current head, the right-hand side of equation 128 is modified to add $\frac{\bar{S}_{ske_{nb}}^{k-1}A_n b_{0_{nb}}}{t-t_{old}}\left(\hat{\sigma}_{c_n}'-\hat{\sigma}'^{\,t_{old}}\right)\frac{\partial S_{F_n}^{*\,k-1}}{\partial h_n}$ as a third term. In this case, this term would be added as a third term to equation 127 and as a third term inside the parentheses of equation 128.

Delay interbed system compaction

The contribution of delay interbed systems to the groundwater flow equation is a simple function of the head in the aquifer and the head in delay interbed cell i and NC. Because the head in delay interbed cells is solved separately from the groundwater flow equation, interbed heads are considered fixed when the groundwater flow equation is solved. The derivative of equation 104 with respect to h_n is

$$\frac{\partial Q_{D_{nb}}^{k-1}}{\partial h_n}=-n_{equiv}\frac{4K_{zz}'A_n}{\Delta z}. \quad (129)$$

The fully implicit form of the Newton-Raphson formulation for the contribution of delay interbed system nb in cell n in the form of equation 2-30 in Langevin and others (2017) is

$$\frac{\partial Q_{D_{nb}}^{k-1}}{\partial h_n}h_n^k=-Q_{D_{nb}}^{k-1}+\frac{\partial Q_{D_{nb}}^{k-1}}{\partial h_n}h_n^{k-1}. \quad (130)$$

Substitution of equations 104 and 129 into equation 130 results in

$$\left[-n_{equiv} \frac{4K'_{zz} A_n}{\Delta z} \right] h_n^k = -n_{equiv} \frac{2K'_{zz} A_n}{\Delta z} \left(H_{NC}^{k-1} + H_1^{k-1} - 2h_n^{k-1} \right) + \left[-n_{equiv} \frac{4K'_{zz} A_n}{\Delta z} \right] h_n^{k-1}. \quad (131)$$

Simplification of equation 131 results in

$$\left[-n_{equiv} \frac{4K'_{zz} A_n}{\Delta z} \right] h_n^k = -n_{equiv} \frac{2K'_{zz} A_n}{\Delta z} \left(H_{NC}^{k-1} + H_1^{k-1} \right), \quad (132)$$

which is equal to equation 105 and indicates additional terms are not needed to complete the Newton-Raphson formulation for the contribution of delay interbed systems to the groundwater flow equation.

Water Compressibility

To reduce the need to recalculate compaction in coarse-grained sediments in aquifers and fine-grained sediments in no-delay interbeds multiple times per outer iteration for water compressibility, thicknesses and porosities are considered constant during an outer iteration, and the analytical derivative of equation 106 is used. The derivative of equation 106 with respect to h_n, assuming $\check{S}^{\star}_{F_n}$ is calculated using the previous head, is

$$\frac{\partial Q_{WC_n}^{k-1}}{\partial h_n} = -\frac{WC_n^{k-1}}{t - t_{old}} S_{F_n}^{* \, k-1} - \frac{WC_n^{k-1}}{t - t_{old}} \frac{\partial S_{F_n}^{* \, k-1}}{\partial h_n} h_n^{k-1}, \quad (133)$$

The fully implicit form of the Newton-Raphson formulation for the contribution of water compressibility in cell n in the form of equation 2-30 in Langevin and others (2017) is

$$\frac{\partial Q_{WC_n}^{k-1}}{\partial h_n} h_n^k = -Q_{WC_n}^{k-1} + \frac{\partial Q_{WC_n}^{k-1}}{\partial h_n} h_n^{k-1}. \quad (134)$$

Substitution of equations 106 and 133 into equation 134 results in

$$\begin{aligned}
\left(-\frac{WC_n^{k-1}}{t - t_{old}} S_{F_n}^{* \, k-1} - \frac{WC_n^{k-1}}{t - t_{old}} h_n^{k-1} \frac{\partial S_{F_n}^{* \, k-1}}{\partial h_n} \right) h_n^k = \\
-\frac{WC_n^{k-1}}{t - t_{old}} \check{S}^{\star}_{F_n} h_n^{t_{old}} + \frac{WC_n^{k-1}}{t - t_{old}} h_n^{k-1} \\
+ \left(-\frac{WC_n^{k-1}}{t - t_{old}} S_{F_n}^{* \, k-1} - \frac{WC_n^{k-1}}{t - t_{old}} h_n^{k-1} \frac{\partial S_{F_n}^{* \, k-1}}{\partial h_n} \right) h_n^{k-1}.
\end{aligned} \quad (135)$$

Simplification of equation 135 results in

$$\left(-\frac{WC_n^{k-1}}{t - t_{old}} S_{F_n}^{* \, k-1} - \frac{WC_n^{k-1}}{t - t_{old}} h_n^{k-1} \frac{\partial S_{F_n}^{* \, k-1}}{\partial h_n} \right) h_n^k =$$

$$- \frac{WC_n^{k-1}}{t - t_{old}} \check{S}_{F_n}^{\star} h_n^{t_{old}} + \left(-\frac{WC_n^{k-1}}{t - t_{old}} h_n^{k-1} \frac{\partial S_{F_n}^{* \, k-1}}{\partial h_n} \right) h_n^{k-1}. \tag{136}$$

The $\frac{WC_n^{k-1}}{t - t_{old}} S_{F_n}^{* \, k-1}$ and $\frac{WC_n^{k-1}}{t - t_{old}} \check{S}_{F_n}^{\star} h_n^{t_{old}}$ terms in equation 136 are subtracted from the diagonal of the coefficient matrix and the right-hand side of the groundwater flow equation during the standard formulation, respectively. The Newton-Raphson formulation is completed by augmenting the coefficient matrix with the second term on the right-hand side of equation 133 and adding the product of the second term on the right-hand side of equation 133 and the current head to the right-hand side of the groundwater flow equation. In cases where $\check{S}_{F_n}^{\star}$ in equation 106 is calculated using the current head, $\frac{WC_n^{k-1}}{t - t_{old}} h_n^{t_{old}} \frac{\partial S_{F_n}^{* \, k-1}}{\partial h_n}$ is added as a third term on the right-hand side of equation 133. In this case, this term would be added as a third term in the parentheses on the left-hand and right-hand sides of equation 136.

Solution of Delay Interbeds Systems

A system of equations for the one-dimensional column of cells shown in figure 5*A* can be expressed in matrix form (eq. 98). To simplify the assembly of the delay bed system of equations, delay beds are solved in terms of specific discharge (q) instead of volumetric discharge (Q) by eliminating the cell area terms from the delay bed flow equations. The initial effective stress ($\hat{\sigma}'^{t_{old}}$) is set based on initial stress conditions calculated from specified initial or steady-state aquifer heads and specified delay interbed heads.

The system of equations describing flow in delay beds is solved as part of the outer iteration formulation step of the Iterative Model Solver (IMS) package (Hughes and others, 2017) prior to formulating the system of the equations for each GWF model cell. Similar to the approach used to solve the three-dimensional groundwater flow equation, the one-dimensional vertical groundwater flow equation (eq. 77) for each column of delay interbed cells is solved using an outer iteration loop that resolves nonlinearities in the equation coefficients and an inner solution step that solves the assembled linear equation. The linear equations for flow in delay interbeds are solved using a tridiagonal direct method (Thomas, 1949). Delay interbed cell terms that are added to the **A** matrix and **r** vector are presented below.

Standard Formulation

The standard formulation available in MODFLOW 6 can be applied to confined problems and water-table problems where cells representing delay interbed cells do not completely dewater during the simulation. Although equations 38 and 39 are nonlinear, the nonlinearity may be mild enough to allow for the use of the standard formulation to assemble delay interbed cell terms.

Delay interbed cell-to-cell specific flow

The specific flow across the top and bottom faces of an interior delay interbed cell for the interior cells ($1 < i < NC$), based on equation 78, is

$$q_{DB_i}^k = K_{zz}' \frac{H_{i-1}^k - H_i^k}{\Delta z_0} + K_{zz}' \frac{H_{i+1}^k - H_i^k}{\Delta z_0}, \tag{137}$$

where Δz_0 is the initial thickness of each delay interbed cell (L) and indicates that the delay interbed cell thickness used to calculate specific flow terms across the top and bottom faces of the cell is constant. Rearranging equation 137 to move terms dependent on the current value of H to the left-hand side of the one-dimensional vertical groundwater flow equation results in

$$-\frac{2K_{zz}'}{\Delta z_0} H_i^k + \frac{K_{zz}'}{\Delta z_0} H_{i-1}^k + \frac{K_{zz}'}{\Delta z_0} H_{i+1}^k. \tag{138}$$

The coefficients in the first term in equation 138 are added to the diagonal for cell i. The coefficients in the second and third terms in equation 138 are added to the $i-1$ and $i+1$ off-diagonals for cell i, respectively. For delay interbed cell $i = 1$, the specific discharge across the top and bottom faces, based on equations 80 and 81 is

$$q_{DB_1}^k = K_{zz}' \frac{H_2^k - H_1^k}{\Delta z_0} + K_{zz}' \frac{h_n^{k-1} - H_1^k}{\frac{\Delta z_0}{2}}. \tag{139}$$

Rearranging equation 139 to move terms dependent on the current value of H to the left-hand side of the one-dimensional vertical groundwater flow equation results in

$$-\frac{3K'_{zz}}{\Delta z_0}H_1^k + \frac{K'_{zz}}{\Delta z_0}H_2^k = -\frac{2K'_{zz}}{\Delta z_0}h_n^{k-1}. \tag{140}$$

The coefficients in the first term on the left-hand side of equation 140 are added to the diagonal for cell 1 and the coefficients in the second term on the left-hand side are added to the off-diagonal for interbed cell 1. The term on the right-hand side of equation 140 is added to the right-hand side of equation 98 for interbed cell 1. For delay interbed cell $i = NC$, the flow across the top and bottom faces based on equations 79 and 82 is

$$q_{DB\,NC}^k = K'_{zz}\frac{H_{NC-1}^k - H_{NC}^k}{\Delta z_0} + K'_{zz}\frac{h_n^{k-1} - H_{NC}^k}{\frac{\Delta z_0}{2}}. \tag{141}$$

Rearranging equation 141 to move terms dependent on the current value of H to the left-hand side of the one-dimensional vertical groundwater flow equation results in

$$-\frac{3K'_{zz}}{\Delta z_0}H_{NC}^k + \frac{K'_{zz}}{\Delta z_0}H_{NC-1}^k = -\frac{2K'_{zz}}{\Delta z_0}h_n^{k-1}. \tag{142}$$

The first term on the left-hand side of equation 142 is added to the diagonal for cell NC, and the second term on the left-hand side is added to the off-diagonal for interbed cell NC. The term on the right-hand side of equation 142 is added to the right-hand side of equation 98 for interbed cell NC.

Delay interbed cell compaction

The contribution of delay interbed compaction to the one-dimensional vertical groundwater flow equation based on equation 84 is

$$\begin{aligned}
q_{STO_i}^k = &\frac{\Delta z_0}{t - t_{old}}\left[S_{F_i}^{k-1}\bar{S}_{sk_i}^{k-1}\left(\hat{\sigma}_i^{k-1} - H_i^k + zb_i - \hat{\sigma}'_{c_i}\right) + \check{S}_{F_i}\bar{S}_{ske_i}^{k-1}\left(\hat{\sigma}'_{c_i} - \hat{\sigma}_i'^{t_{old}}\right)\right] + \\
&\frac{\Delta z_0}{t - t_{old}}S_{F_i}^{k-1}\bar{S}_{sk_i}^{k-1}\left(H_i^{k-1} - \bar{H}_i^{k-1}\right).
\end{aligned} \tag{143}$$

where q_{STO} is the specific flow from storage for the delay interbed cell (LT^{-1}) and $\bar{H}$ is the linear corrected head for the delay interbed cell (L). The saturated cell fraction for delay interbed cell i is introduced to generalize equation 84 for water-table conditions. S_{F_i} is 1 for all values of H if GWF cell n is defined to be non-convertible (confined) in the MODFLOW 6 storage package. The second term on the right-hand side of equation 143 is a flow correction term that corrects q_{STO} when H_i is less than zb_i. Rearranging equation 143 to move terms dependent on the current value of H to the left-hand side of the equation and all other terms to the right-hand side of the equation results in

$$
-\frac{\Delta z_0}{t - t_{old}} S_{F_i}^{k-1} \bar{S}_{sk_i}^{k-1} H_i^k =
$$
$$
-\frac{\Delta z_0}{t - t_{old}} \left[S_{F_i}^{k-1} \bar{S}_{sk_i}^{t} \left(\hat{\sigma}_i^{k-1} + z b_i - \hat{\sigma}_{c_i}' \right) + \check{S}_{F_i} \bar{S}_{ske_i}^{t} \left(\hat{\sigma}_{c_i}' - \hat{\sigma}_i'^{t_{old}} \right) \right] \quad (144)
$$
$$
-\frac{\Delta z_0}{t - t_{old}} S_{F_i}^{k-1} \bar{S}_{sk_i}^{k-1} \left(H_i^{k-1} - \bar{H}_i^{k-1} \right).
$$

The coefficients in the term on the left-hand side and terms on the right-hand side of equation 144 are added to the diagonal and the right-hand side of equation 98 for cell i.

Water compressibility

The contribution of delay interbed water compressibility to the one-dimensional vertical groundwater flow equation based on equation 85 is

$$
q_{WC_i}^k = \frac{1}{t - t_{old}} \left(\check{S}_{F_i} S_{sw_i}^{t_{old}} b_i^{t_{old}} H_i^{t_{old}} - S_{F_i}^{k-1} S_{sw_i}^{k-1} b_i^{k-1} H_i^k \right), \quad (145)
$$

where q_{WC} is the specific flow from water compressibility for the delay interbed cell (LT^{-1}). The saturated cell fraction for delay interbed cell i is introduced to generalize equation 85 for water-table conditions. S_{F_i} is 1 for all values of H if GWF cell n is defined to be nonconvertible (confined) in the MODFLOW 6 storage package. Rearranging equation 145 to move terms dependent on the current value of H to the left-hand side of the equation and all other terms to the right-hand side of the equation results in

$$
-\frac{1}{t - t_{old}} \left(S_{F_i}^{k-1} S_{sw_i}^{k-1} b_i^{k-1} \right) H_i^k = -\frac{1}{t - t_{old}} \left(\check{S}_{F_i} S_{sw_i}^{t_{old}} b_i^{t_{old}} H_i^{t_{old}} \right). \quad (146)
$$

The coefficients in the term on the left-hand side and terms on the right-hand side of equation 146 are added to the diagonal and the right-hand side of equation 98 for cell i.

Newton-Raphson Formulation

The Newton-Raphson formulation is used for delay interbeds when the Newton-Raphson formulation option is enabled in MODFLOW 6. The Newton-Raphson formulation option can improve model convergence for highly nonlinear problems. The Newton-Raphson formulation for delay interbed cells uses quadratically smoothed saturated fraction (eq. 113) and corrected heads (eq. 115) like the CSUB package terms used to solve the three-dimensional groundwater flow equation. Delay interbeds are solved as part of the MODFLOW 6 outer iteration formulation step and derivative terms are directly calculated instead of being added as correction terms added to the standard formulation terms already added to the coefficient matrix $\mathbf{A}$ and the right-hand side vector $\mathbf{r}$.

Delay interbed cell-to-cell specific flow

The derivatives of equation 137 with respect to H_i, H_{i-1}, and H_{i+1} are

$$\frac{\partial q_{DB}}{\partial H_i} = -\frac{2K'_{zz}}{\Delta z_0},$$ (147a)

$$\frac{\partial q_{DB}}{\partial H_{i-1}} = \frac{K'_{zz}}{\Delta z_0}, \quad \text{and}$$ (147b)

$$\frac{\partial q_{DB}}{\partial H_{i+1}} = \frac{K'_{zz}}{\Delta z_0}.$$ (147c)

The fully implicit form of the Newton-Raphson formulation for the contribution of delay interbed cells $i - 1$ and $i + 1$ to delay interbed cell i in the form of equation 2-30 in Langevin and others (2017) is

$$\frac{\partial q_{DB}}{\partial H_i} H_i^k + \frac{\partial q_{DB}}{\partial H_{i-1}} H_{i-1}^k + \frac{\partial q_{DB}}{\partial H_{i+1}} H_{i+1}^k = -q_{DB_i}^{k-1} + \frac{\partial q_{DB}}{\partial H_i} H_i^{k-1} + \frac{\partial q_{DB}}{\partial H_{i-1}} H_{i-1}^{k-1} + \frac{\partial q_{DB}}{\partial H_{i+1}} H_{i+1}^{k-1}.$$ (148)

The first derivative term on the left-hand side of equation 148 is added to the diagonal for cell i. The second and third derivative terms on the left-hand side of equation 148 are added to the $i - 1$ and $i + 1$ off-diagonals for cell i. The sum of the terms on the right-hand side of equation 150 is zero, so nothing is added to r_i. For delay interbed cell 1, the derivatives of equation 139 with respect to H_1 and H_2 are

$$\frac{\partial q_{DB}}{\partial H_1} = -\frac{3K'_{zz}}{\Delta z_0} \quad \text{and}$$ (149a)

$$\frac{\partial q_{DB}}{\partial H_2} = \frac{K'_{zz}}{\Delta z_0}.$$ (149b)

The fully implicit form of the Newton-Raphson formulation for the contribution of delay interbed cell $i + 1$ to delay interbed cell i in the form of equation 2-30 in Langevin and others (2017) is

$$\frac{\partial q_{DB}}{\partial H_1} H_1^k + \frac{\partial q_{DB}}{\partial H_2} H_2^k = -q_{DB_1}^{k-1} + \frac{\partial q_{DB}}{\partial H_1} H_1^{k-1} + \frac{\partial q_{DB}}{\partial H_2} H_2^{k-1}.$$ (150)

Equation 150 can be simplified using equation 139 to

$$\frac{\partial q_{DB}}{\partial H_1} H_1^k + \frac{\partial q_{DB}}{\partial H_2} H_2^k = -\frac{2K'_{zz}}{\Delta z_0} h_n^{k-1},$$ (151)

which is equal to equation 140. The first derivative term on the left-hand side of equation 151 is added to the diagonal for cell 1. The second derivative term on the left-hand side of equation 151 is added to the $i + 1$ off-diagonal for cell 1. The entire right-hand side of equation 151 is added to r_1. Similarly, for delay interbed cell NC, the derivatives of equation 141 with respect to H_{NC} and H_{NC-1} are

$$\frac{\partial q_{DB}}{\partial H_{NC}} = -\frac{3K'_{zz}}{\Delta z_0} \quad \text{and} \tag{152a}$$

$$\frac{\partial q_{DB}}{\partial H_{NC-1}} = \frac{K'_{zz}}{\Delta z_0}. \tag{152b}$$

The fully implicit form of the Newton-Raphson formulation for the contribution of delay interbed cell $NC-1$ to delay interbed cell i in the form of equation 2-30 in Langevin and others (2017) is

$$\frac{\partial q_{DB}}{\partial H_{NC}} H_{NC}^k + \frac{\partial q_{DB}}{\partial H_{NC-1}} H_{NC-1}^k = -q_{DB_{NC}}^{k-1} + \frac{\partial q_{DB}}{\partial H_{NC}} H_{NC}^{k-1} + \frac{\partial q_{DB}}{\partial H_{NC-1}} H_{NC-1}^{k-1}. \tag{153}$$

Equation 153 can be simplified using equation 141 to

$$\frac{\partial q_{DB}}{\partial H_{NC}} H_{NC}^k + \frac{\partial q_{DB}}{\partial H_{NC-1}} H_{NC-1}^k = -\frac{2K'_{zz}}{\Delta z_0} h_n^{k-1}, \tag{154}$$

which is equal to equation 142. The first derivative term on the left-hand side of equation 154 is added to the diagonal for cell NC. The second derivative term on the left-hand side of equation 154 is added to the $i-1$ off-diagonal for cell NC. The entire right-hand side of equation 154 is added to r_{NC}.

Delay interbed cell compaction

Simplification of equation 143 removes the current delay interbed cell value (H_i^{k-1}) and results in

$$q_{STO_i}^k = \frac{\Delta z_0}{t - t_{old}} \left[S_{F_i}^{*\,k-1} \bar{S}_{sk_i}^{k-1} \left(\hat{\sigma}_i^{k-1} - \bar{H}_i^{*\,k-1} + zb_i - \hat{\sigma}'_{c_i} \right) + \check{S}_{F_i}^{\star} \bar{S}_{ske_i}^{k-1} \left(\hat{\sigma}'_{c_i} - \hat{\sigma}'^{\,t_{old}}_i \right) \right], \tag{155}$$

where $\bar{H}^{\star}$ is the quadratically smoothed corrected head in a delay interbed cell. The derivative of equation 155 with respect to H_i, assuming $\bar{S}_{sk_i}$ and $\bar{S}_{ske_i}$ are head-independent and $\check{S}_{F_i}^{\star}$ is calculated using the previous head is

$$\frac{\partial q_{STO_i}^{k-1}}{\partial H_i} = -\frac{\Delta z_0}{t - t_{old}} S_{F_i}^{*\,k-1} \bar{S}_{sk_i}^{k-1} \frac{\partial \bar{H}_i^{*\,k-1}}{\partial \bar{H}_i} + \frac{\Delta z_0}{t - t_{old}} \bar{S}_{sk_{nb}}^{k-1} \left(\hat{\sigma}_n^{k-1} - \bar{H}_i^{k-1} + zb_n - \hat{\sigma}'_{c_n} \right) \frac{\partial S_{F_i}^{*\,k-1}}{\partial H_i}. \tag{156}$$

The fully implicit form of the Newton-Raphson formulation for the contribution of compaction to delay interbed cell i in the form of equation 2-30 in Langevin and others (2017) is

$$\frac{\partial q_{STO_i}^{k-1}}{\partial H_i} H_i^k = -q_{STO_i}^{k-1} + \frac{\partial q_{STO_i}^{k-1}}{\partial H_i} H_i^{k-1}. \tag{157}$$

The derivative term on the left-hand side of equation 157 is added to the diagonal for cell i. The entire right-hand side of equation 157 is added to r_i. In cases where $\check{S}_{F_i}^{\star}$ in equation 155 is calculated using the current head, the right-hand side of equation 156 is modified to add $\frac{\Delta z_0}{t - t_{old}} \bar{S}_{ske_i}^{k-1} \left(\hat{\sigma}'_{c_i} - \hat{\sigma}'^{\,t_{old}}_i \right) \frac{\partial S_{F_i}^{*\,k-1}}{\partial H_i}$ as a third term.

Delay interbed cell water compressibility

The derivative of equation 145 with respect to H_i, assuming $\check{S}^{\star}_{F_i}$ is calculated using the previous head, is

$$\frac{\partial q^{k-1}_{WC_i}}{\partial H_i} = -\frac{1}{t - t_{old}} S^{\star\,k-1}_{F_i} S^{k-1}_{sw_i} b^{k-1}_i - \frac{1}{t - t_{old}} S^{k-1}_{sw_i} b^{k-1}_i H^{k-1}_i \frac{\partial S^{\star\,k-1}_{F_i}}{\partial H_i}. \tag{158}$$

The fully implicit form of the Newton-Raphson formulation for the contribution of water compressibility to delay interbed cell i in the form of equation 2-30 in Langevin and others (2017) is

$$\frac{\partial q^{k-1}_{WC_i}}{\partial H_i} H^k_i = -q^{k-1}_{WC_i} + \frac{\partial q^{k-1}_{WC_i}}{\partial H_i} H^{k-1}_i. \tag{159}$$

The derivative term on the left-hand side of equation 159 is added to the diagonal for cell i. The entire right-hand side of equation 159 is added to r_i. In cases where $\check{S}^{\star}_{F_i}$ in equation 145 is calculated using the current head, the right-hand side of equation 158 is modified to add $\frac{1}{t-t_{old}} S^{t_{old}}_{sw_i} b^{t_{old}}_i H^{t_{old}}_i \frac{\partial S^{\star\,k-1}_{F_i}}{\partial H_i}$ as a third term.

Applicability and Limitations of the CSUB Package

The package documented in this report is designed for simulation of basin-scale aquifer-system compaction coupled with groundwater flow. Calculations are of vertical displacement, and use of the package, therefore, is not recommended for applications in which significant horizontal components of displacement might exist. Burbey (2001) found that small changes in porosity resulting from horizontal strain can yield large quantities of water in close proximity to pumping wells. As a result, inappropriate applications include small-scale deformation in the vicinity of a pumping well and deformation in areas around geologic discontinuities that cause abrupt lateral variations in the thickness of compressible sediments.

As previously described, the CSUB package can account for changing geostatic stress and, by default, does not treat elastic and inelastic storage properties as constants. The SUB-WT package (Leake and Galloway, 2007) has the ability to track changing geostatic stresses, but the SUB package (Hoffmann and others, 2003) does not. Unlike the SUB-WT package, this package can account for the delay in release of water from compressible interbeds, as can be done with the SUB package (Hoffmann and others, 2003). The Terzaghi elastoplastic model used in the CSUB package does not account for secondary consolidation (creep) that can occur in sediments, especially those with a high amount of organic material, in the absence of effective stress changes. The CSUB package includes an option ("head-based" option) to hold the geostatic stress constant, which results in effectively the same interbed formulation as available in the SUB package. The capabilities of the CSUB package allow this package to be applied to any problem that used either the SUB or SUB-WT package available in previous versions of MODFLOW. The CSUB package is also applicable to both regular and irregular model grids.

The approach used in the CSUB package assumes the compaction of individual interbeds to be small compared with that of the original interbed thickness. The specified interbed thicknesses are not adjusted to account for interbed compaction, nor are model layer thicknesses adjusted to account for compaction occurring in individual model layers. Users should carefully evaluate the final strain in coarse- and fine-grained sediments; summaries of strain rates exceeding 1 percent are printed to the model listing files, and summaries of strain rates can be saved for coarse-grained cells and all fine-grained interbeds. If updating material properties and the thickness of compressible sediments or the porosity reduces to values less than or equal to zero, the program will terminate with an error. Possible remedies for this situation are to reduce the model time step or to reduce the inelastic or elastic storage properties. Reducing the model time step may also be required for water-table simulations where head changes are a large percentage of the cell thickness. Vertical cell discretization may also need to be evaluated for water-table simulations where head changes are a large percentage of the cell thickness.

The effective stress can become negative in cells located at the top of the model when the water level exceeds land surface. Because the effective stress is used to calculate inelastic and elastic skeletal specific storage values (eqs. 38 and 39), negative effective stresses result in nonphysical skeletal specific storage values. The model will terminate with an error if negative effective stresses are calculated during the simulation. Because groundwater seepage to the land surface occurs in shallow aquifers when groundwater levels exceed land surface, negative effective stress values can be eliminated by adding drains to these cells using the drain (DRN) or unsaturated zone flow (UZF) packages. Negative effective stress values can also be eliminated by increasing the thickness of cells located at the top of the model.

The delay interbed formulation was developed using the assumption that multiple interbeds can be represented as a system of interbeds and the results from a single equivalent delay interbed can be used to calculate the cumulative contribution of each delay interbed to the cell. For delay interbeds, simulated results should be carefully evaluated if the groundwater head drops below the top of the cell because in this case, the calculated elastic- and inelastic-specific storage values are no longer calculated relative to the center of the cell.

For cells with a water table and containing coarse-grained sediments or fine-grained sediments in no-delay interbeds, it is assumed that sediments above the water table do not supply water from storage to the saturated

flow system or experience compaction (for example, fine-grained interbeds in the unsaturated zone in fig. 1). Helm (1984) presented an approach to simulating continued compaction of fine-grained sediments stranded by a declining water table, but this approach has not been implemented in the CSUB package.

Another assumption is that interbeds are distributed uniformly in the vertical dimension within each model cell. In this way, the calculated effective stress at the center of the saturated thickness of a cell is representative of average conditions for the entire cell, and effective stress changes at the bottom of a cell are representative of effective stress changes throughout the cell. If interbeds are distributed nonuniformly in the vertical or simulated stress conditions are not representative of conditions in individual interbeds, additional vertical discretization may be needed to characterize the vertical bedding. Additional vertical discretization may also be required to accurately simulate stress changes in aquifers and confining beds containing a water table. Further, it also assumed that the horizontal area of the interbed is equal to the horizontal area of the GWF cell containing the interbed. Increased horizontal discretization will be required if the horizontal area of an individual interbed is less than the horizontal cell area.

Compressible sediments in aquifer systems may occur as interbeds within aquifers or as extensive confining units adjacent to aquifers (fig. 1). In basin-scale groundwater models, simulation of flow and storage changes in individual interbeds within aquifers is impractical because of difficulties in mapping the interbeds and also because high-resolution finite-difference grids would be required to represent small geologic features. As was presented by Hoffmann and others (2003), this report documents an approach to simulating flow and storage changes in groups or systems of interbeds. Flow and storage changes in individual confining units, however, can be simulated in basin-scale flow models. To simulate flow and storage changes in a confining unit, one model layer or a number of model layers must be used to represent each confining unit (Hoffmann and others, 2003, fig. 5C). Increasing the number of model layers increases the accuracy in simulating flow and storage changes in a confining unit but also increases computation and computer storage requirements (Leake and others, 1994). One system of interbeds should be used for each layer in a confining unit.

In MODFLOW 6, each stress period may be either steady state or transient. The ability to mix steady-state and transient stress periods in a single simulation allows users to set up an initial steady-state stress period that simulates steady-state predevelopment conditions and subsequent stress periods that simulate post-development transient conditions. The CSUB package does not make any calculations in steady-state stress periods, but the heads calculated by the model for a steady-state stress period are relevant to calculations made by the package for subsequent transient stress periods. If any stress periods other than the first are steady state, the CSUB package will terminate with an error. Simulations are allowed in which the first stress period is steady-state and subsequent stress periods are transient, or in which all stress periods are transient. If the first stress period is steady state, the heads at the end of the stress period are used to calculate initial stress conditions for the second stress period. If the first stress period is transient, initial heads are used to calculate initial stress conditions. Specified preconsolidation stresses are set equal to calculated initial effective stress values in interbeds with specified values that are less than calculated initial effective stress values.

References Cited

Abidin, H.Z., Andreas, H., Gumilar, I., and Brinkman, J.J., 2015, Study on the risk and impacts of land subsidence in Jakarta: Proceedings of the International Association of Hydrological Sciences, v. 372, p. 115–120, accessed October 11, 2019, at https://doi.org/10.5194/piahs-372-115-2015.

Alam, M., 1996, Subsidence of the Ganges—Brahmaputra Delta of Bangladesh and Associated Drainage, Sedimentation and Salinity Problems, *in* Milliman, J.D., and Haq, B.U., eds., Sea-Level Rise and Coastal Subsidence: Causes, Consequences, and Strategies: Dordrecht, Springer Netherlands, p. 169–192, accessed March 3, 2021, at https://doi.org/10.1007/978-94-015-8719-8_9.

Amelung, F., Galloway, D.L., Bell, J.W., Zebker, H.A., and Laczniak, R.J., 1999, Sensing the ups and downs of Las Vegas—InSAR reveals structural control of land subsidence and aquifer-system deformation: Geology, v. 27, no. 6, p. 483–486, accessed October 11, 2019, at https://doi.org/10.1130/0091-7613(1999)027<0483:STUADO>2.3.CO;2.

Bawden, G.W., Thatcher, W., Stein, R.S., Hudnut, K.W., and Peltzer, G., 2001, Tectonic contraction across Los Angeles after removal of groundwater pumping effects: Nature, v. 412, no. 6849, p. 812–815, accessed October 11, 2019, at https://doi.org/10.1038/35090558.

Burbey, T.J., 2001, Storage coefficient revisited—Is purely vertical strain a good assumption?: Groundwater, v. 39, no. 3, p. 458–464, accessed October 11, 2019, at https://doi.org/10.1111/j.1745-6584.2001.tb02330.x.

Eggleston, J., and Pope, J., 2013, Land subsidence and relative sea-level rise in the southern Chesapeake Bay region: U.S. Geological Survey Circular 1392, 30 p., accessed October 11, 2019, at https://doi.org/10.3133/cir1392.

Faunt, C.C., Sneed, M., Traum, J., and Brandt, J.T., 2016, Water availability and land subsidence in the Central Valley, California, USA: Hydrogeology Journal, v. 24, no. 3, p. 675–684, accessed October 11, 2019, at https://doi.org/10.1007/s10040-015-1339-x.

Fetter, C.W., 1988, Applied hydrogeology (2nd ed.): New York, Macmillan Publishing Company, 592 p.

Freeze, R.A., and Cherry, J.A., 1979, Groundwater: Englewood Cliffs, N.J., Prentice-Hall, 604 p.

Galloway, D.L., and Burbey, T.J., 2011, Regional land subsidence accompanying groundwater extraction: Hydrogeology Journal, v. 19, no. 8, p. 1459–1486, accessed October 11, 2019, at https://doi.org/10.1007/s10040-011-0775-5.

Galloway, D.L., Jones, D.R., and Ingebritsen, S.E., 1999, Land subsidence in the United States: U.S. Geological Survey Circular 1182, 175 p., accessed October 11, 2019, at https://doi.org/10.3133/cir1182.

Helm, D.C., 1975, One-dimensional simulation of aquifer system compaction near Pixley, California: 1. Constant parameters: Water Resources Research, v. 11, no. 3, p. 465–478, accessed October 11, 2019, at https://doi.org/10.1029/WR011i003p00465.

Helm, D.C., 1976, One-dimensional simulation of aquifer system compaction near Pixley, California: 2. Stress-Dependent Parameters: Water Resources Research, v. 12, no. 3, p. 375–391, accessed October 11, 2019, at https://doi.org/10.1029/WR012i003p00375.

Helm, D.C., 1984, Latrobe Valley subsidence predictions–the modeling of time-dependent ground movement due to groundwater withdrawal: Joint Report of Fuel Department and Design Engineering and Environment Department, State Electricity Commission of Victoria, Melbourne, 2 vols.

Heywood, C.E., 1998, Piezometric-extensometric estimations of specific storage in the Albuquerque basin, New Mexico, *in* Borchers, J.W., ed., Land Subsidence Case Studies and Current Research: Proceedings of the Dr. Joseph F. Poland Symposium on Land Subsidence: Association of Engineering Geologists Special Publication no. 8, p. 435–440.

Hoffmann, J., Zebker, H.A., Galloway, D.L., and Amelung, F., 2001, Seasonal subsidence and rebound in Las Vegas Valley, Nevada, observed by synthetic aperture radar interferometry: Water Resources Research, v. 37, no. 6, p. 1551–1566, accessed October 11, 2019, at https://doi.org/10.1029/2000WR900404.

Hoffmann, J., Leake, S.A., Galloway, D.L., and Wilson, A.M., 2003, MODFLOW-2000 Ground-Water Model—User Guide to the Subsidence and Aquifer-System Compaction (SUB) Package: U.S. Geological Survey Open-File Report 03–233, 44 p., accessed June 27, 2017, at https://pubs.usgs.gov/of/2003/ofr03-233/.

Hughes, J.D., Langevin, C.D., and Banta, E.R., 2017, Documentation for the MODFLOW 6 framework: U.S. Geological Survey Techniques and Methods, book 6, chap. A57, 36 p., accessed August 4, 2017, at https://doi.org/10.3133/tm6A57.

Ingebritsen, S.E., and Galloway, D.L., 2014, Coastal subsidence and relative sea level rise: Environmental Research Letters, v. 9, no. 9, article 091002, accessed March 1, 2021, at https://doi.org/10.1088/1748-9326/9/9/091002.

Jacob, C.E., 1940, On the flow of water in an elastic artesian aquifer: Eos, Transactions American Geophysical Union, v. 21, no. 2, p. 574–586, accessed October 6, 2019, at https://doi.org/10.1029/TR021i002p00574.

Jorgensen, D.G., 1980, Relationships between basic soils-engineering equations and basic ground-water flow equations: U.S. Geological Survey Water-Supply Paper 2064, 40 p., accessed September 22, 2017, at https://pubs.usgs.gov/wsp/2064/report.pdf.

Kasmarek, M.C., and Johnson, M.R., 2013, Groundwater withdrawals 1976, 1990, and 2000–10 and land-surface-elevation changes 2000–10 in Harris, Galveston, Fort Bend, Montgomery, and Brazoria Counties, Texas: U.S. Geological Survey Scientific Investigations Report 2013–5034, 17 p., accessed October 11, 2019, at https://doi.org/10.3133/sir20135034.

Kavetski, D., and Kuczera, G., 2007, Model smoothing strategies to remove microscale discontinuities and spurious secondary optima in objective functions in hydrological calibration: Water Resources Research, v. 43, no. 3, accessed March 1, 2021, at https://doi.org/10.1029/2006WR005195.

Kooi, H., and Erkens, G., 2020, Creep consolidation in land subsidence modelling; integrating geotechnical and hydrological approaches in a new modflow package (sub-cr): Proceedings of the International Association of Hydrological Sciences, v. 382, p. 499–503, accessed Novermber 25, 2020, at https://doi.org/10.5194/piahs-382-499-2020.

Kooi, H., Bakr, M., de Lange, G., den Hann, E., and Erkens, G., 2018, User guide to SUB-CR; a MODFLOW package for land subsidence and aquifer system compaction that includes creep: Deltares internal report 11202275-008, 63 p., accessed November 25, 2020, at http://publications.deltares.nl/11202275_008.pdf.

Langevin, C.D., Hughes, J.D., Provost, A.M., Banta, E.R., Niswonger, R.G., and Panday, S., 2017, Documentation for the MODFLOW 6 Groundwater Flow (GWF) Model: U.S. Geological Survey Techniques and Methods, book 6, chap. A55, 197 p., accessed August 4, 2017, at https://doi.org/10.3133/tm6A55.

Leake, S.A., and Galloway, D.L., 2007, MODFLOW Ground-water model—User guide to the Subsidence and Aquifer-System Compaction Package (SUB-WT) for Water-Table Aquifers: U.S. Geological Survey Techniques and Methods, book 6, chap. A23, 42 p., accessed June 27, 2017, at https://pubs.er.usgs.gov/publication/tm6A23.

Leake, S.A., and Prudic, D.E., 1991, Documentation of a computer program to simulate aquifer-system compaction using the modular finite-difference ground-water flow model: U.S. Geological Survey Techniques of Water-Resources Investigations, book 6, chap. A2, 68 p., accessed June 27, 2017, at https://pubs.er.usgs.gov/publication/twri06A2.

Leake, S.A., Leahy, P.P., and Navoy, A.S., 1994, Documentation of a computer program to simulate transient leakage from confining units using the modular finite-difference ground-water flow model: U.S. Geological Survey Open-File Report 94–59, 70 p., accessed October 11, 2019, at https://doi.org/10.3133/ofr9459.

Lu, Z., and Danskin, W.R., 2001, InSAR analysis of natural recharge to define structure of a ground-water basin, San Bernardino, California: Geophysical Research Letters, v. 28, no. 13, p. 2661–2664, accessed October 11, 2019, at https://doi.org/10.1029/2000GL012753.

Meyer, W.R., and Carr, J.E., 1979, A digital model for simulation of ground-water hydrology in the Houston area, Texas: U.S. Geological Survey Open-File Report 79–677, 23 p., accessed October 11, 2019, at https://doi.org/10.3133/ofr79677.

Minderhoud, P. S.J., Erkens, G., Pham, V.H., Bui, V.T., Erban, L., Kooi, H., and Stouthamer, E., 2017, Impacts of 25 years of groundwater extraction on subsidence in the Mekong delta, Vietnam: Environmental Research Letters, v. 12, no. 6, article 064006, accessed October 11, 2019, at https://doi.org/10.1088/1748-9326/aa7146.

Neuman, S.P., Preller, C., and Narasimhan, T.N., 1982, Adaptive explicit-implicit quasi three-dimensional finite element model of flow and subsidence in multiaquifer systems: Water Resources Research, v. 18, no. 5, p. 1551–1561, accessed November 19, 2021, at https://doi.org/10.1029/WR018i005p01551.

Niswonger, R.G., Panday, S., and Ibaraki, M., 2011, MODFLOW-NWT, A Newton formulation for MODFLOW-2005: U.S. Geological Survey Techniques and Methods, book 6, chap. A37, 44 p., accessed June 27, 2017, at https://pubs.er.usgs.gov/publication/tm6A37.

Panday, S., Langevin, C.D., Niswonger, R.G., Ibaraki, M., and Hughes, J.D., 2013, MODFLOW-USG version 1—An unstructured grid version of MODFLOW for simulating groundwater flow and tightly coupled processes using a control volume finite-difference formulation: U.S. Geological Survey Techniques and Methods, book 6, chap. A45, 66 p., accessed June 27, 2017, at https://pubs.usgs.gov/tm/06/a45/.

Poland, J.F., and Davis, G.H., 1969, Land subsidence due to withdrawal of fluids: Reviews in Engineering Geology, v. 2, p. 187–270, accessed August 28, 2017, at https://doi.org/http://dx.doi.org/10.1130/REG2.

Poland, J.F., and Ireland, R.L., 1985, Land Subsidence in the Santa Clara Valley, California, as of 1980: Mechanics of Aquifer Systems: U.S. Geological Survey Open-File Report 84–818, 93 p., accessed October 11, 2019, at https://doi.org/10.3133/ofr84818.

Poland, J.F., Ireland, R.L., Lofgren, B.E., and Pugh, R.G., 1975, Land subsidence in the San Joaquin Valley, California, as of 1972: U.S. Geological Survey Professional Paper 437–H, 78 p., accessed October 11, 2019, at https://doi.org/10.3133/pp437H.

Riley, F.S., 1969, Analysis of borehole extensometer data from Central California: International Association of Scientific Hydrology Publication 89, v. 2, p. 423–431.

Shirzaei, M., Freymueller, J., Törnqvist, T.E., Galloway, D.L., Dura, T., and Minderhoud, P.S., 2020, Measuring, modelling and projecting coastal land subsidence: Nature Reviews Earth & Environment, v. 2, nos. 40–58, 19 p., accessed November 19, 2021, at https://doi.org/10.1038/s43017-020-00115-x.

Sneed, M., Brandt, J.T., and Solt, M., 2014, Land subsidence, groundwater levels, and geology in the Coachella Valley, California, 1993-2010: U.S. Geological Survey Scientific Investigations Report 2014–5075, 62 p., accessed October 11, 2019, at https://doi.org/10.3133/sir20145075.

Sneed, M., Brandt, J.T., and Solt, M., 2018, Land subsidence along the California Aqueduct in west-central San Joaquin Valley, California, 2003–10: U.S. Geological Survey Scientific Investigations Report 2018–5144, 67 p., accessed October 11, 2019, at https://doi.org/10.3133/sir20185144.

Šuklje, L., 1957, The analysis of the consolidation process by the isotache method, *in* Proceedings of the 4th International Conference on Soil Mechanics and Foundation Engineering, London, v. 1, p. 200–206.

Terzaghi, K., 1925, Erdbaumechanik Auf Bodenphysikalischer Grundlage: Wien, Austria, Deuticke, 399 p.

Theis, C.V., 1935, The relation between the lowering of the piezometric surface and the rate and duration of discharge of a well using ground-water storage: Eos, Transactions American Geophysical Union, v. 16, no. 2, p. 519–524, accessed November 19, 2021, at https://doi.org/10.1029/TR016i002p00519.

Thomas, L., 1949, Elliptic problems in linear differential equations over a network: Watson Scientific Computing Laboratory, Columbia University, New York, 71 p.

Williamson, A.K., Prudic, D.E., and Swain, L.A., 1989, Ground-water flow in the Central Valley, California: U.S. Geological Survey Professional Paper 1401–D, 127 p., accessed October 11, 2019, at https://doi.org/10.3133/pp1401D.

Wilson, A.M., and Gorelick, S., 1996, The effects of pulsed pumping on land subsidence in the Santa Clara Valley, California: Journal of Hydrology, v. 174, nos. 3–4, p. 375–396, accessed October 11, 2019, at https://doi.org/10.1016/0022-1694(95)02722-X.

Appendix 1.   List of Mathematical Symbols

The following is a list of mathematical symbols used in this report.

Symbol	Description	Dimension	Definition
∂	partial differential operator	-	
d	implicit differential operator	-	
Δ	finite difference operator	-	
δ_{ij}	Kronecker delta function	-	
M	Mass unit (kg, lb, etc.)	M	
L	Length unit (m, ft, etc.)	L	
T	Time unit (sec, day, etc.)	T	
(n, m)	connection between cells n and m	-	eq. 96
e subscript	elastic (non-virgin) compaction or storage property	-	eq. 33
i subscript	delay interbed column cell number	-	eq. 77
j subscript	number of interbed grouped into a delay interbed system	-	eq. 88
n subscript	cell number	-	eq. 46
m subscript	cell number	-	eq. 46
nb subscript	interbed number	-	eq. 64
v subscript	inelastic (virgin) compaction or storage property	-	eq. 31
k superscript	current iteration	-	eq. 99
t superscript	time	T	eq. 40
t_{old} superscript	time at the end of the previous time step	T	eq. 40
$\vee$ superscript	variable calculated using the current (h^{k-1}) or previous ($h^{t_{old}}$) head	-	eq. 99
$*$ superscript	quadratically smoothed variable	-	eq.113
$\wedge$ superscript	stress in terms of the height of an equivalent column of water	L	eq. 17
$\in$	mathematical symbol that denotes membership in a set	-	eq. 52
$\sum_{m \in \eta_n}$	summation over cells connected to cell n	-	eq. 96
$\sum_{\substack{m \in \eta_n \\ zb_m = zt_n}}$	summation over cells connected to cell m, excluding cells where $zb_m \neq zt_n$	-	eq. 52
α	compressibility of the aquifer or confining unit	MLT^{-2}	eq. 4
$\bar{\alpha}$	one-dimensional (vertical) coefficient of compressibility of the aquifer or confining unit	MLT^{-2}	eq. 26
β	compressibility of water	$LM^{-1}T^2$	eq. 4
ϵ	total vertical strain	-	eq. 43
η_n	cells connected to cell n	-	eq. 52
γ_g	unit weight of sediments	$ML^{-2}T^{-2}$	eq. 13
γ_m	unit weight of moist sediments above the water table	$ML^{-2}T^{-2}$	eq. 12
γ_s	unit weight of saturated sediments	$ML^{-2}T^{-2}$	eq. 12
γ_w	unit weight of water	$ML^{-2}T^{-2}$	eq. 2

List of mathematical symbols used in this report.—Continued

Symbol	Description	Dimension	Definition
Ω	small distance over which the quadratic smoothing occurs	L	eq. 113
ψ	pressure head, in terms of the elevation difference of the water column relative to the piezometer bottom	L	eq. 1
σ'_{ij}	component of the effective stress tensor	$MLT^{-2}L^{-2}$ or L	eq. 10
σ'	vertical component of effective stress	$MLT^{-2}L^{-2}$	eq. 11
$\hat{\sigma}'$	vertical component of effective stress	L	eq. 17
$\bar{\sigma}'$	average effective stress	L	eq. 56
σ_{ij}	component of the total stress tensor	$MLT^{-2}L^{-2}$	eq. 10
σ	vertical component of geostatic stress	$MLT^{-2}L^{-2}$	eq. 11
$\hat{\sigma}$	vertical component geostatic stress	L	eq. 17
$\bar{\sigma}_o$	average geostatic stress in the cells directly overlying cell n or specified load applied to cells with no overlying cells	L	eq. 46
$\hat{\sigma}_{top}$	geostatic stress at the top of the one-dimensional delay interbed column	L	eq. 69
σ'_c	preconsolidation stress	$MLT^{-2}L^{-2}$	eq. 40
$\hat{\sigma}'_c$	preconsolidation stress	L	eq. 64
ρ_w	density of water	ML^{-3}	eq. 2
θ	porosity	-	eq. 4
θ_w	moisture content of sediments in the unsaturated zone	-	eq. 13
A	horizontal area of a aquifer, confining unit, or cell	L^2	eq. 9
$\mathbf{A}$	coefficient matrix	L^2T^{-1} or LT^{-1}	eq. 98
A_Ω	defined as $\frac{1}{1-\Omega}$	L^{-1}	eq. 113
b	thickness of a control volume, aquifer, confining unit, or cell	L	eq. 23
b_0	initial thickness of a aquifer, confining unit, or cell	L	eq. 25
b_{e0}	initial thickness of elastic coarse-grained materials	L	eq. 59
b_{equiv}	equivalent delay interbed thickness	L	eq. 88
b_j	the thickness of delay interbed j in delay interbed system nb	L	eq. 88
b_m	thickness of moist/unsaturated sediments	L	eq. 12
b_s	thickness of saturated sediments	L	eq. 12
C_c	compression index	-	eq. 27
C_r	recompression index	-	eq. 33
$C_{n,m}$	the conductance between connected cells n and m	L^2T^{-1}	eq. 96
db or Δb	compaction	L	eq. 23
db_e or Δb_e	elastic compaction	L	eq. 33
db_v or Δb_v	inelastic compaction	L	eq. 32
de	change in void ratio	-	eq. 22
de_v or Δe_v	inelastic change in the void ratio	-	eq. 31
e	void ratio	-	eq.19
e_0	initial void ratio	-	eq.25
f_{e0}	initial fraction of elastic coarse-grained materials in a cell	-	eq. 60
g	gravitational acceleration	LT^{-2}	eq. 2
G_m	specific gravity of moist sediments in a cell	-	eq. 46
G_s	specific gravity of saturated sediments in a cell	-	eq. 46

List of mathematical symbols used in this report.—Continued

Symbol	Description	Dimension	Definition
h	hydraulic head	L	eq. 1
$\bar{h}$	linear corrected head	L	eq. 49
$\bar{h}^\star$	quadratically smoothed corrected head	L	eq. 115
H	head in a delay interbed cell	L	eq. 72
$\bar{H}$	linear corrected head in a delay interbed cell	L	eq. 71
$\bar{H}^\star$	quadratically smoothed corrected head in a delay interbed cell	L	eq. 155
dh or Δh	head change in an aquifer or confining unit	L	eq. 9
K'_{zz}	vertical hydraulic conductivity of the delay interbed	LT^{-1}	eq. 68
n_{equiv}	delay interbed flow multiplication factor	-	eq. 89
nd	total number of delay interbeds	-	eq. 97
nnd	total number of no-delay interbeds	-	eq. 93
N	number of individual delay interbeds with similar vertical hydraulic diffusivity	-	eq. 88
NC	number of cells in a one-dimensional delay interbed column	-	page 42
P	sum of external-stress coefficients for cell	L^2T^{-1}	eq. 96
p	fluid pore pressure	$MLT^{-2}L^{-2}$	eq. 2
q	specific discharge	LT^{-1}	page 42
q_{DB}	specific flow between two delay interbed cells or the GWF cell containing the interbed	LT^{-1}	eq. 137
q_{STO}	specific flow for storage in a delay interbed cell	LT^{-1}	eq. 143
q_{WC}	specific flow resulting from water compressibility	LT^{-1}	eq. 145
Q	volumetric discharge	L^3T^{-1}	page 42
Q_D	volumetric flow rate between a delay interbed system and the cell containing the interbed	L^3T^{-1}	eq. 90
Q_{DB}	volumetric flow rate between two delay interbed cells	L^3T^{-1}	eq. 77
Q_n	sum of external-stress coefficients for cell n	L^3T^{-1}	eq. 96
$Q_n^\star$	sum of CSUB package terms for cell n that are calculated using $h^{t_{old}}$ or h^t from the previous iteration	L^3T^{-1}	eq. 96
Q_{ND}	flow from no-delay interbeds	L^3T^{-1}	eq. 67
Q_{sk}	flow from coarse-grained sediments	L^3T^{-1}	eq. 63
Q_{Sy}	flow from contribution from specific yield	L^3T^{-1}	eq. 97
Q_{STO}	volumetric flow rate from storage in a delay interbed cell	L^3T^{-1}	eq. 77
Q_{TOTAL}	total volumetric flow rate from storage	L^3T^{-1}	eq. 97
Q_{WC}	volumetric storage change resulting from the compression of water	L^3T^{-1}	eq. 77
$\mathbf{r}$	vector containing known components of the continuity equation	L^3T^{-1} or LT^{-1}	eq. 98
S	storage coefficient (storativity)	-	eq. 6
S_F	linear saturated fraction of the aquifer or confining unit	-	eq. 99
$\hat{S}_F$	linear saturated cell fraction based on the current (h_n^{k-1}) or previous ($h_n^{t_{old}}$) head	-	eq. 99
S_F^*	quadratically smoothed saturated fraction of cell	-	eq. 113
S_s	specific storage	L^{-1}	eq. 4
S_{sk}	skeletal specific storage	L^{-1}	eq. 4
S_{sw}	water specific storage	L^{-1}	eq. 4

List of mathematical symbols used in this report.—Continued

Symbol	Description	Dimension	Definition
S_{ske}	elastic skeletal specific storage value	L^{-1}	eq. 37
$\bar{S}_{ske}$	average elastic skeletal specific storage value	-	eq. 62
S_{skv}	inelastic skeletal specific storage value	L^{-1}	eq. 36
S_y	specific yield	-	eq. 8
$SC2$	"secondary storage capacity" for a cell	L^2	eq. 96
dv or Δv	thickness of aquifer, confining unit, or cell (fully saturated)	L	eq. 6
V_t	volume of total volume of a control volume	L^3	eq. 5
V_s	volume of solids in a control volume	L^3	eq. 5
V_v	volume of voids in a control volume	L^3	eq. 5
dV_w or ΔV_w	volume of water added or released from storage	(L^3)	eq. 9
WC	water compressibility coefficient	L^2	eq. 86
$\mathbf{x}$	vector of unknown heads	L	eq. 98
z	elevation head measured at the bottom of a piezometer	L	eq. 1
$\bar{z}$	center of the saturated thickness in a cell	L	eq. 56
z_{offset}	offset of the center of a delay interbed cell from the center of the interbed	L	eq. 73
dz or Δz	thickness of each delay interbed cell	L	eq. 79
Δz_0	initial thickness of each delay interbed cell	L	eq. 73
zb	bottom of a aquifer, confining unit, or cell	L	eq. 7
$\overline{zb}$	bottom of a delay interbed cell relative to the center of the saturated thickness of cell containing the delay interbed	L	eq. 73
zt	top of a aquifer, confining unit, or cell	L	eq. 7
$\overline{zt}$	top of a delay interbed cell relative to the center of the saturated thickness of cell containing the delay interbed	L	eq. 73

Hughes and others—**Documentation for the Skeletal Storage, Compaction, and Subsidence (CSUB) Package of MODFLOW 6**—Techniques and Methods 6—A62